Article

Spatiotemporal Characteristics of Dryness/Wetness in the Wine Regions of China from 1981 to 2015

Xiaojuan Yang [1,2,*], Ning Yao [3], Wei Hu [4], Xingjie Ji [5], Qingzu Luan [6], Yuan Liu [1,2], Wei Bai [1,2], Di Chen [1,2] and Buchun Liu [1,2,*]

[1] Institute of Environment and Sustainable Development in Agriculture, Chinese Academy of Agricultural Sciences, Beijing 100081, China; liuyuan@caas.cn (Y.L.); baiwei@caas.cn (W.B.); chendi@caas.cn (D.C.)
[2] National Engineering Laboratory of Efficient Crop Water Use and Disaster Reduction, Chinese Academy of Agricultural Sciences, Beijing 100081, China
[3] College of Water Resources and Architectural Engineering, Northwest Agriculture and Forestry University, Yangling, Xianyang 712100, China; yaoning@nwafu.edu.cn
[4] New Zealand Institute for Plant and Food Research Ltd., Christchurch 8140, New Zealand; wei.hu@plantandfood.co.nz
[5] Henan Institute of Meteorological Sciences, Zhengzhou 450003, China; jixingjie2004@aliyun.com
[6] Beijing Municipal Climate Center, Beijing 100089, China; qzluan@bj.cma.gov.cn
* Correspondence: yangxiaojuan@caas.cn (X.Y.); liubuchun@caas.cn (B.L.)

Abstract: China has a marked continental monsoon climate characterized by dry and wet hazards that have destructive impacts on grape yields and quality. The purpose of this study was to analyze the spatiotemporal characteristics of dryness/wetness in the wine regions of China and explore the links between these variations and large-scale climatic factors. The crop-specific standardized precipitation evapotranspiration index (SPEI) was used to characterize the dryness/wetness using meteorological data collected at 168 meteorological stations located in or near the wine regions from 1981–2015. Results showed that most wine regions of China experienced a wetting trend. The drought and wet event characteristics were region- and site-specific. The main wine regions of China (e.g., Xinjiang, Helan Mountain and Hexi Corridor) were characterized by relatively high drought severity; the extreme drought frequencies of the three regions were higher as well (11.5%, 3.3%, and 3.6%, respectively). Xinjiang was also characterized by a high wetness severity and an extremely high wetness frequency of 16%, but the wetness severity decreased over time. A 4–6-year periodical oscillation was commonly detected over the wine regions. The dryness/wetness characteristics were highly associated with the Southern Oscillation Index, Niño 3.4 and the Indian Ocean Dipole, with highest correlation coefficients of −0.40, 0.36 and 0.43 at lag times of 11, 8, and 11 months, respectively. The serious dry and wet events that occurred in 2001 and 1998, respectively, were speculated to be associated with anomalous atmospheric circulation patterns. These results can be used to inform grapevine stakeholders at various levels (e.g., farmer and industry) for developing strategies to mitigate and adapt dryness/wetness events in the wine regions of China. It is expected that the approach proposed in this study can also be applicable to wine regions of other countries.

Keywords: China; wine region; SPEI; drought; wet; climatic factors

1. Introduction

Grapevines (*Vitis vinifera* L.) are an important crop with 7.8 million hectares of cultivated land and an annual production of 67.6 million tons worldwide [1]. According to International Organization of Vine and Wine (OIV) statistics, in 2014, China had the second-largest vineyard surface area, the seventh-largest wine production, and the fifth-largest wine consumption in the world, with values of 796,000 ha, 11,600,000 hL and 15,500,000 hL, respectively [2]. The effects of climatic conditions were found to explain 24.1% of the wine variances [3]. In contrast to most of the wine regions around the world that benefit

from a Mediterranean climate, China has a marked continental monsoon climate that is characterized by dry and wet hazards [4]. Drought events have deleterious impacts on viticulture around the world, and the occurrence of unfavorable abundant rainfall during ripening can lead to severe disease outbreaks and epidemics that cause losses ranging from 40 to 90% [5,6]. Reductions in fruit quality and fruit yield cause substantial economic losses to the grape industry. Hence, there is a need to fully recognize the spatiotemporal characteristics of dryness and wetness in the wine regions of China.

Many indices have been developed to characterize and monitor droughts using variable climatic and hydrologic data [7–9]. Among these indices, the standardized precipitation index (SPI) and standardized precipitation evapotranspiration index (SPEI) are the indices most commonly used to monitor dry and wet conditions [10–15]. The SPI characterizes water deficit and surplus conditions [16], provides a better representation of wetness and dryness [17], and can be applied to any location on a month-based timescale [17]. While the SPI is recommended as an optimal drought index because the required parameters are simple, only precipitation is considered in this index, making it, to some extent, specifically applicable to meteorological drought [12] and preventing it from reflecting drought conditions caused by warming. The SPEI was proposed as an improved drought index compared to the SPI; it describes the deviation degrees of dry and wet conditions by standardizing the difference between precipitation and potential evapotranspiration [13]; the SPEI is suitable for studying the effects of global warming on drought severity [10]. Guo et al. [18] analyzed the spatiotemporal drought characteristics in Central Asia from 1966 to 2015 using the SPEI and found that Central Asia showed an overall wetting trend with a switch to a drying trend since 2003; additionally, a common, significant 16–64-month periodical oscillation was detected. Gao et al. [12] found that water resources are expected to increase under global warming, which may alleviate the water scarcity issue on the Loess Plateau from 2001 to 2050. Polong et al. [13] studied the temporal and spatial evolution of the SPEI in the Tana River Basin of Kenya, and the results showed that the period between 1960 and 1980 was dominated by dry events, while wet events were dominant in the period between 1990 and 2000 [13].

However, in the SPEI forms used in the studies described above, the calculated potential evapotranspiration (ET_0) referred to water lost to the atmosphere by evaporation from the soil surface and by transpiration from a reference surface [19]; this calculation method cannot represent a specific crop. The crop evapotranspiration (ETc) can be calculated by multiplying the ET_0 by a crop coefficient (Kc) that varies predominantly with specific crop characteristics, and the resulting metric can represent the evapotranspiration from a specific crop surface [19]. Thus, calculating the SPEI using the ETc instead of the ET_0 can serve to assess the dryness and wetness of specific crop-planting areas.

The reasons for the occurrence of dryness/wetness are extremely complex because dryness/wetness relates not only to the climatology of a specific region but also to different atmospheric circulation mechanisms. Among these atmospheric mechanisms, the El Niño–Southern Oscillation (ENSO) event is considered as the dominant climate mode in the equatorial Pacific with considerable effects on the global climate [20]. With the occurrence of ENSO-related warm and cold events, extreme weather disasters, such as drought and flooding, have occurred in most parts of the world. Precipitation in China changes under the influence of ENSO events [21]. The Indian Ocean dipole (IOD), an important mode of interannual variability in the tropical Indian Ocean, has been proposed as another significant factor influencing rainfall over China. Past studies have also found that the IOD was primarily associated with dryness and wetness [22]. Therefore, it is necessary to analyze the effect of these large-scale climatic factors on the dryness/wetness of wine regions in China.

The general objective of this study is, therefore, to comprehensively determine the spatiotemporal characteristics of dryness and wetness in the wine regions of China based on the SPEI from 1981–2015 and the relationship of the SPEI with large-scale climatic factors. Specifically, the objectives of this study are (1) to detect the temporal variations and spatial

trends in the SPEI using grapevine evapotranspiration in the wine regions of China; (2) to identify drought and wet events and reveal the characteristics of dryness and wetness in the wine regions of China based on run theory and the modified Mann-Kendall (MMK) trend test; and (3) to reveal the dryness/wetness periodicity and its relationship with climatic factors using bivariate and multiple wavelet coherence analysis. The findings of this study are promising for providing a valuable scientific reference to mitigating drought and wetness risks in the wine regions of China.

2. Data and Methodology

2.1. Study Area and Datasets

Eleven wine regions within 21 provincial areas of the entire wine regions of mainland China (EMC) were chosen to conduct this research; these wine regions were primarily delimited according to meteorological geographic divisions and administrative divisions [4]. A total of 168 weather stations located in or near these 11 wine regions (Jing-Jin-Ji: JJJ; Northeast: NE; Inner Mongolia: IM; Hexi Corridor: HXC; Helan Mountain, HLM; Xinjiang: XJ; Loess Plateau: LP; Ancient Yellow River: AYR; Shandong: SD; Southwest: SW and Special: S) were selected to analyze the dryness and wetness conditions in the wine regions of China (Figure 1). Authoritative drought events were collected from Ding [23]. The records were stated on a yearly scale from 1950–2000. Drought events after 2000 were also mentioned but incomplete. According to Ding [23], droughts occurred almost every year (except in 1964 and 1970) in different regions and different seasons. Extreme nationwide droughts occurred in 1961, 1965, 1972, 1978, 1986, 1988, 1992, 1994, 1997, 1999 and 2000. The observed weather variables, including the daily precipitation (P), relative humidity (RH), minimum temperature (T_{min}), mean temperature (T_{mean}) and maximum temperatures (T_{max}), wind speed at 2 m (U_2), and sunshine hours (n) data recorded over the 1981–2015 period were collected from the Meteorological Data Sharing Service Network in China following strict quality control. The quality and reliability of the data were cross-examined using nonparametric tests, including the Kendall autocorrelation test and Mann-Whitney homogeneity test [24]. The precipitation increased from the northwest to the southeast, and the mean temperature was higher in Xinjiang, Ancient Yellow River, Shandong, and Special regions and lower in the Northeast region during the grapevine growing stage.

The following large-scale climate indices covering the period from 1981 to 2015 were chosen to explore the possible relationships between climatic factors and dryness/wetness variabilities in the wine regions of China: ENSO was considered using the Niño 3.4 SST index and Southern Oscillation Index in this study, as derived from the National Oceanic and Atmospheric Administration (NOAA) Earth System Research Laboratory (https://www.esrl.noaa.gov/, accessed on 9 September 2020), and Indian Ocean Dipole data were obtained from the National Climate Center of China (http://cmdp.ncc-cma.net/Monitoring/cn_index_130.php, accessed on 9 September 2020).

2.2. Computation of the SPEI

The ET_0 (reference crop evapotranspiration, mm·d^{-1}) was estimated using the Food and Agricultural Organization (FAO)-56 Penman-Monteith equation [25], which can be expressed as follows:

$$ET_0 = \frac{0.408\Delta(R_n - G) + \gamma\frac{900}{T+273}U_2(e_d - e_a)}{\Delta + \gamma(1 + 0.34U_2)} \tag{1}$$

where Δ is the vapor pressure slope curve (KPa·°C^{-1}), R_n is the net radiation at the crop surface (MJ·m^{-2}·d^{-1}), G is the soil heat flux density (MJ·m^{-2}·d^{-1}) (assumed to be zero based on the FAO-56 recommendation that the magnitude of the daily or ten-day soil heat flux beneath a grass reference surface may be ignored because it is relatively small), T is the mean daily air temperature at a height of 2 m (°C), U_2 is the wind speed at 2 m

above the ground (m·S^{-1}), e_d is the saturation vapor pressure (KPa), e_a is the actual vapor pressure (KPa), and γ is the psychrometric constant (KPa·°C^{-1}).
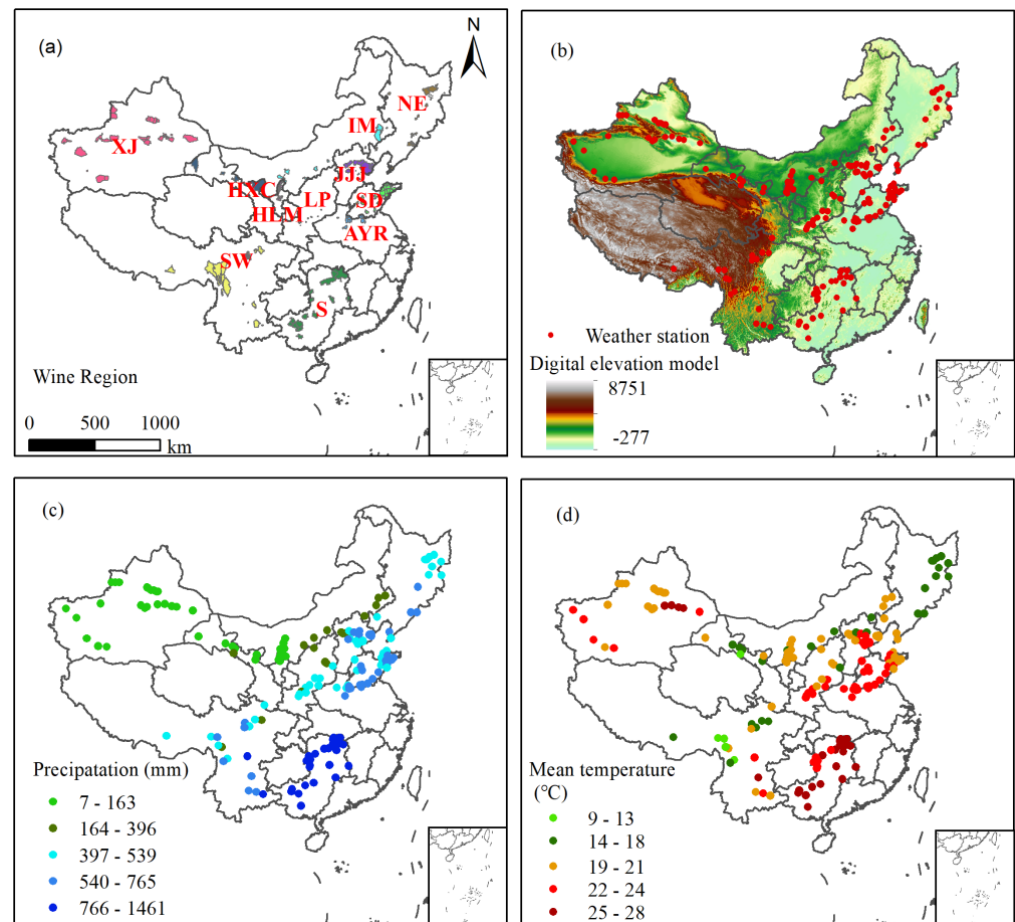

Figure 1. Spatial distribution of wine regions (**a**), related weather stations (**b**), precipitation (**c**) and mean temperature (**d**) during the grapevine growth period in China.

The ET_C (crop evapotranspiration) was determined by the crop coefficient and reference evapotranspiration procedure. Next, the ET_0 outputs were multiplied by the crop coefficient (K_C) to estimate the crop evapotranspiration as follows:

$$ET_C = K_C \times ET_0 \tag{2}$$

The monthly crop coefficients for grapevine from April to September have been reported to be 0.3, 0.45, 0.52, 0.76, 0.70, and 0.60, respectively [26]. The crop-specific SPEI was calculated using the P and ET_C series to indicate drought and wetness in the wine regions. The computation procedure of the SPEI followed the method outlined by Vicente-Serrano et al. [14]: (1) First, the ET_0 is estimated at the monthly timescale using Equation (1); (2) next, the accumulation of the water condition D (P-ET_C) is determined at the 1- and 6-month time scales; and (3) D is normalized into a log-logistic probability distribution to obtain the SPEI series using Equations (3) and (4):

$$F(x) = \left[1 + \left(\frac{\alpha}{x - \gamma} \right)^{\beta} \right]^{-1} \tag{3}$$

$$SPEI = W - \frac{c_0 + c_1 W + c_2 W^2}{1 + d_1 W + d_2 W^2 + d_3 W^3} \tag{4}$$

where $F(x)$ is the probability distribution function of the D series and α, β and γ are the scale, shape, and origin parameters, respectively [14,27]. For $P(D) \leq 0.5$, $W = \sqrt{-2lnP(D)}$ and $P(D) = 1 - F(x)$; for $P(D) > 0.5$, $P(D)$ is replaced by $1 - P(D)$, and the sign of the SPEI is reversed.

The growth period of grapevine lasts from 1 April to 30 September. The 1-month-scale SPEI calculated from April to September (SPEI1) was used to reflect the evolution and characteristics of the short-term water condition (the difference between precipitation and grapevine evapotranspiration) during the grapevine growth period in the wine regions of China. The 6-month-scale SPEI (SPEI6-Sep) was used to reflect the long-term water condition of the whole grapevine growth period in each studied wine region.

2.3. Identification and Characterization of Drought/Wet Events

Run theory is one of the most frequently used methods to characterize drought and wet events. A run is defined as a portion of the variable time series in which all values are below a selected threshold [28,29]. Runs can be both positive and negative which indicate the wet and drought events respectively.

The SPEI1 was used to identify drought and wet events during grapevine growth. It was reported to capture the historical drought and wet events efficiently [9]. A drought event was thought to have started when the SPEI1 fell below -1 and ended when the SPEI1 rose above 0. A wet event started when the SPEI1 rose above 1 and ended when the SPEI1 fell below 0. A drought event corresponded to a negative run, while a wet event corresponded to a positive run. Once drought and wet events were defined, they could be characterized in terms of the drought/wet duration (DD/WD), drought/wet severity (DS/WS), drought/wet intensity (DI/WI), and drought/wet peak (DP/WP) based on run theory. The definition of these characteristics was listed on the following Table 1.

Table 1. The definition of drought/wet characteristics.

Drought/Wet Characteristics	Definition
drought/wet duration (DD/WD)	The number of months between the drought/wet initiation time and the termination time
drought/wet severity (DS/WS)	The positive sum of the SPEI values determined during a drought/wet event.
drought/wet intensity (DI/WI)	The average SPEI value during the drought/wet duration and was calculated by dividing the drought/wet severity by the drought/wet duration.
drought/wet peak (DP/WP)	The absolute lowest/highest SPEI value recorded at the time of peak drought/wet conditions during an event.
drought/wet frequency (DF/WF)	The number of drought/wet event occurrences during the study period divided by the studied years in the spatial study

In order to investigate the temporal and spatial drought/wet event characteristics, a series of drought/wet event indices were calculated based on the drought/wet events identified by the run theory in each region and at each station separately. The spatial characteristics of drought/wet events at individual stations were calculated using the simple arithmetic mean of the corresponding characteristics of individual drought/wet events (DD/WD, DS/WS, DI/WI, and DP/WP, respectively).

2.4. Trend Test

The nonparametric Mann-Kendall (MK) test is one of the most widely used nonparametric tests in climate studies for detecting trends in time series and is highly recommended for general use by the World Meteorological Organization. However, the MK method tends to underestimate the sample variance because it suffers from time-series correlation. The modified nonparametric Mann–Kendall (MMK) method [30], which adds a correction factor to the original variance computation based on the effective or equivalent sample size (ESS) to avoid the effect of temporal data autocorrelation [31,32], is applied to analyze the tendencies of the dryness/wetness indices.

The modified MMK statistic Z^* was calculated using the following equations:

$$Z^* = \frac{Z}{\sqrt{n^s}} \tag{5}$$

$$n^s = 1 + \frac{2}{n(n-1)(n-2)} \sum_{j=1}^{n-1} (n-j)(n-j-1)(n-j-2)r_j \tag{6}$$

where n^s is the calibration factor, j is the lag number, and r_j is the autocorrelation function of the time series.

2.5. Bivariate and Multiple Wavelet Coherence

The wavelet method is a common tool that has been widely used to untangle scale-specific and localized relationships for the assessment of nonstationary processes in the geosciences. Bivariate wavelet coherence is a special case of multiple wavelet coherence [33,34]. Both analyses are based on smoothed auto- and cross-wavelet power spectra series [35–37]. We only briefly introduce the equations related to the bivariate wavelet coherence and multiple wavelet coherence analyses in this section; readers can refer to previous studies for details [33,34,38–41].

Assuming a response variable Y and multiple predictor variables X ($X = \{X_1, X_2, \ldots, X_q\}$), the multiple wavelet coherence (MWC) at scale s and location τ, $\rho_m^2(s, \tau)$ can be written as follows:

$$\rho_m^2(s, \tau) = \frac{\overset{\leftrightarrow Y,X}{W}(s,\tau)\overset{\leftrightarrow X,X}{W}(s,\tau)^{-1}\overline{\overset{\leftrightarrow Y,X}{W}(s,\tau)}}{\overset{\leftrightarrow Y,Y}{W}(s,\tau)} \tag{7}$$

where $\overset{\leftrightarrow Y,X}{W}(s,\tau)$, $\overset{\leftrightarrow X,X}{W}(s,\tau)$, and $\overset{\leftrightarrow Y,Y}{W}(s,\tau)$ compose the matrices of the smoothed cross-wavelet power spectra between response variable Y and predictor variables X, the matrix of the smoothed auto and cross-wavelet power spectra series among multiple predictor variables X, and the smoothed wavelet power spectrum of response variable Y, respectively. The term $\overline{\overset{\leftrightarrow Y,X}{W}(s,\tau)}$ is a complex conjugate of $\overset{\leftrightarrow Y,X}{W}(s,\tau)$.

When only one predictor variable (e.g., X_1) is included in X, Equation (1) becomes the equation for bivariate wavelet coherence, $\rho_b^2(s, \tau)$, which can be expressed as follows [35,42]:

$$\rho_b^2(s, \tau) = \frac{\overset{\leftrightarrow Y,X_1}{W}(s,\tau)\,\overline{\overset{\leftrightarrow Y,X_1}{W}(s,\tau)}}{\overset{\leftrightarrow X_1,X_1}{W}(s,\tau)\overset{\leftrightarrow Y,Y}{W}(s,\tau)} \tag{8}$$

The wavelet phase between a response variable (Y) and a predictor variable (X_1) is shown as follows:

$$\phi(s, \tau) = \tan^{-1}\left(\text{Im}\left(W^{Y,X_1}(s,\tau)\right)/\text{Re}\left(W^{Y,X_1}(s,\tau)\right)\right) \tag{9}$$

where Im and Re denote the imaginary and real parts of $W^{Y,X_1}(s,\tau)$, respectively.

Both the bivariate wavelet coherence and multiple wavelet coherence were calculated at the 95% significance level using the Monte Carlo method [33,35].

3. Results

3.1. Temporal and Spatial Variations in SPEI

The temporal evolution of the SPEI1 in each wine region is shown in Figure 2a–k. The regional characteristics were obvious based on the linear trend lines. The NE, HXC, LP, and SW regions remained stable or slightly dry, whereas the other regions (JJJ, IM, HLM, XJ,

AYR, SD, and S) became increasingly wet from 1981–2015. Dry and wet climate processes alternated in the entire wine regions of mainland China (EMC) on different time scales from 1981–2015 (Figure 2m). As the timescale decreased, the amplitude and frequency of the fluctuations increased, while the separations between the dryness and wetness intensified. Despite the great detected differences in the fluctuation frequency, the linear trend lines showed similar patterns among different time scales. The SPEI6-Sep and SPEI1 values showed increasing trends, suggesting that a wet trend occurred in the EMC region from 1981 to 2015.

The quantified SPEI trend was listed in Table 1. The results were consistent with the linear lines shown in Figure 2. The SPEI6-Sep and SPEI1 values calculated in each wine region showed the same trends except those obtained for the IM, LP, and SW regions. The SPEI6-Sep and SPEI1 values in the EMC region showed increasing trends. In the NE, HXC, LP, and SW regions, decreasing trends were identified, while the other regions showed increasing trends according to the SPEI1. These results indicated that the NE, HXC, LP, and SW regions experienced drying trends, while the other regions and the EMC experienced wetting trends from 1981–2015.

The spatial distributions of the SPEI1 and SPEI6-Sep trends are mapped in Figure 3. The results showed that the site SPEI trends were consistent with the regional results obtained in SD and AYR; the other SPEI trends were site-specific throughout the rest of the wine regions (Figure 3, Table 2). For example, in NE, the SPEI1 and SPEI6-Sep values obtained at some sites showed increasing trends, while others showed decreasing trends; regionally, a decreasing trend was observed.

3.2. Drought Characteristics

The drought events identified by the SPEI1 were used to analyze the drought trend characteristics. The drought trend characteristics are shown in Figure 4 and exhibited both regional and site specificity. The DS trend was consistent with the DD trend in most wine regions except IM, HLM, LP, S, and EMC; both DD and DS increased in HXC and AYR and decreased in JJJ, NE, XJ, SD, and SW. In LP and S, the DS trend was increasing, but the DD trend was decreasing; the IM region showed the opposite characteristics. A decreasing DD trend was found in EMC. The DI trend was consistent with that of DP in most regions. They decreased in JJJ, HLM, XJ, and LP and increased in HXC, AYR, SW, S, and EMC. NE and SD exhibited increasing DI trends and decreasing DP trends, while IM showed the opposite characteristics. DF decreased in the EMC and in most wine regions, increased only in NE, HCX, HLM, and LP. The drought trend characteristics were also site-specific and differed in each wine region (Figure 4). For example, some sites showed increasing drought trend characteristics in XJ, although a regional decreasing trend was observed in this region.
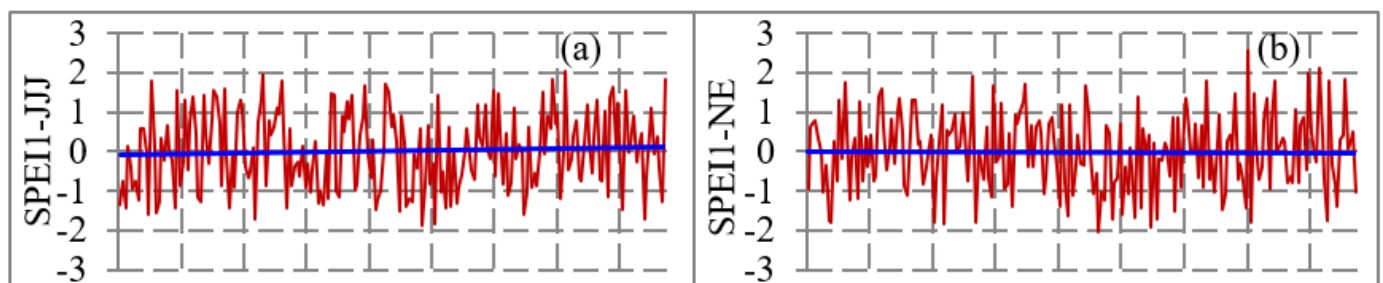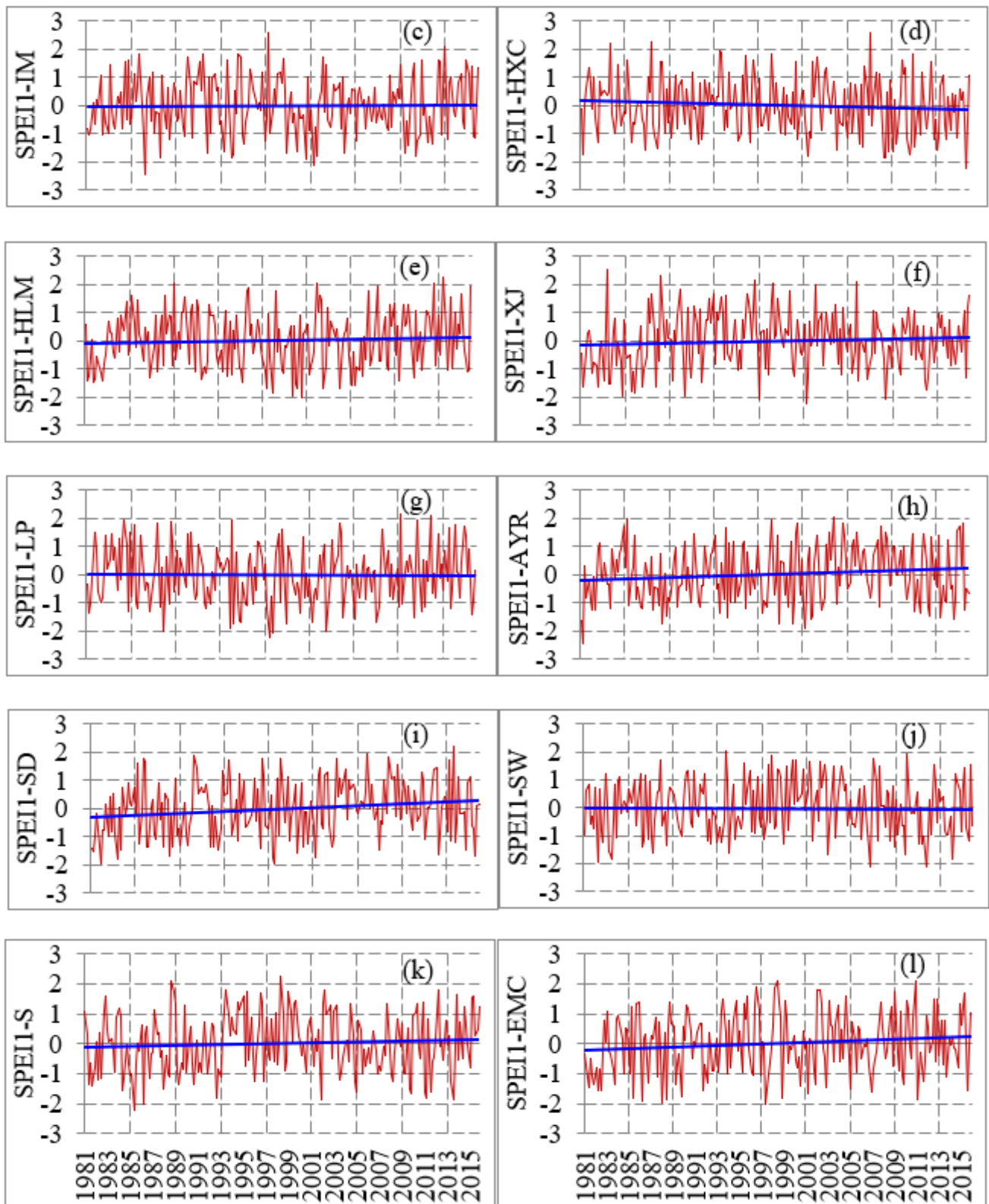

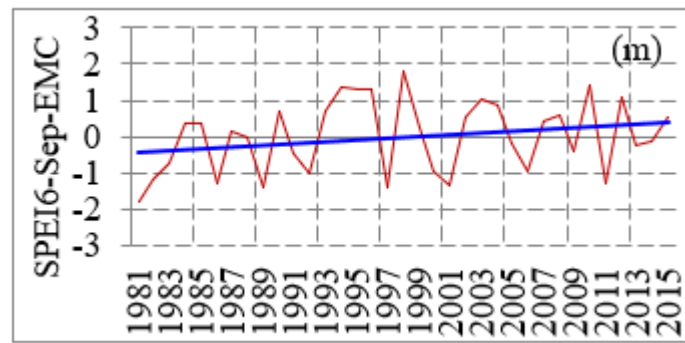**Figure 2.** *Cont.*

Figure 2. *Cont.*

Figure 2. Temporal evolution of the SPEI in the wine regions of China from 1981–2015.
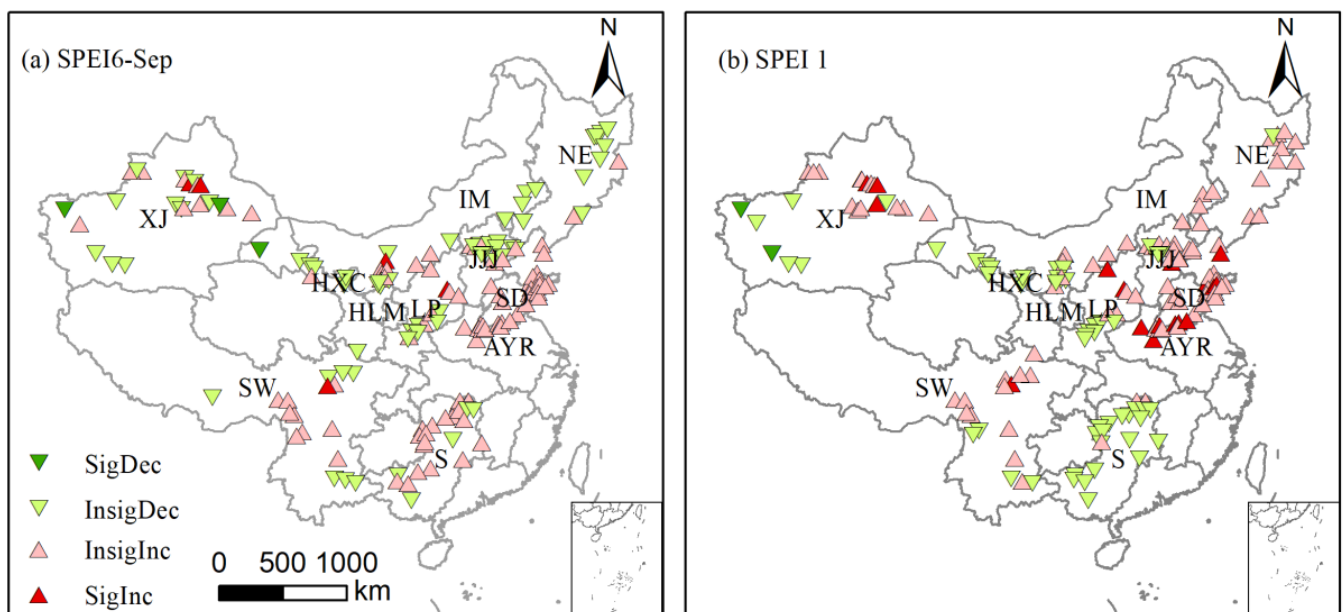

Figure 3. Spatial distributions of the SPEI6-Sep and SPEI1 trends in the wine regions of China. SigDec, InsigDec, InsigInc, and SigInc represent significant decrease, insignificant decrease, insignificant increase, and significant increase trends, respectively.

Table 2. The SPEI6-Sep and SPEI1 trends obtained in the wine regions of China from 1980 to 2015.

	JJJ	NE	IM	HXC	HLM	XJ	LP	AYR	SD	SW	S	EMC
SPEI6-Sep	0.28	−0.44	−0.42	−1.77	1.44	0.14	0.06	1.12	1.61	0.24	1.07	1.72
SPEI1	1.36	−0.36	0.16	−1.78	1.14	1.10	−0.07	1.49	1.82	−0.15	1.19	1.84

The spatial distributions and the regional averages of the obtained drought characteristics are shown in Figure 5. The drought characteristics showed regional features; DS and DD had similar spatial patterns in XJ, HLM, and HXC characterized by relatively high values, while these regions also had relatively low DF values. This result indicated that these regions experienced fewer drought events with longer durations and higher severities. In contrast, the LP and JJJ region suffered from higher DF values but relatively short DDs and lower DSs. The NE region was characterized by a relatively high DF as well as higher DI and DP values. The drought characteristics also showed site-specific features, and greater differences were identified among stations, although no large differences among regions were observed, especially in DI or DP.

Figure 4. The trends of drought severity (DS), drought duration (DD), drought intensity (DI), drought peak (DP), and drought frequency (DF) of the drought events identified by the SPEI1 in the wine regions of China from 1981–2015. SigDec, InsigDec, InsigInc, and SigInc represent significant decrease, insignificant decrease, insignificant increase, and significant increase trends, respectively.

The three levels of drought frequency corresponding to the wine regions of China are listed in Table 3. The number of drought events in different wine regions ranged between 26 and 30. Moderate drought events occurred most often, followed by severe drought events and extreme drought events in each region and in the EMC. The frequency of extreme drought events in XJ was 11.5%, much higher than those obtained in the other regions. No extreme drought events were identified in JJJ, NE, AYR, SD, or S. NE, IM and LP experienced more severe drought events than other regions, and SD, SW, JJJ, and AYR experienced more moderate drought events than other regions.

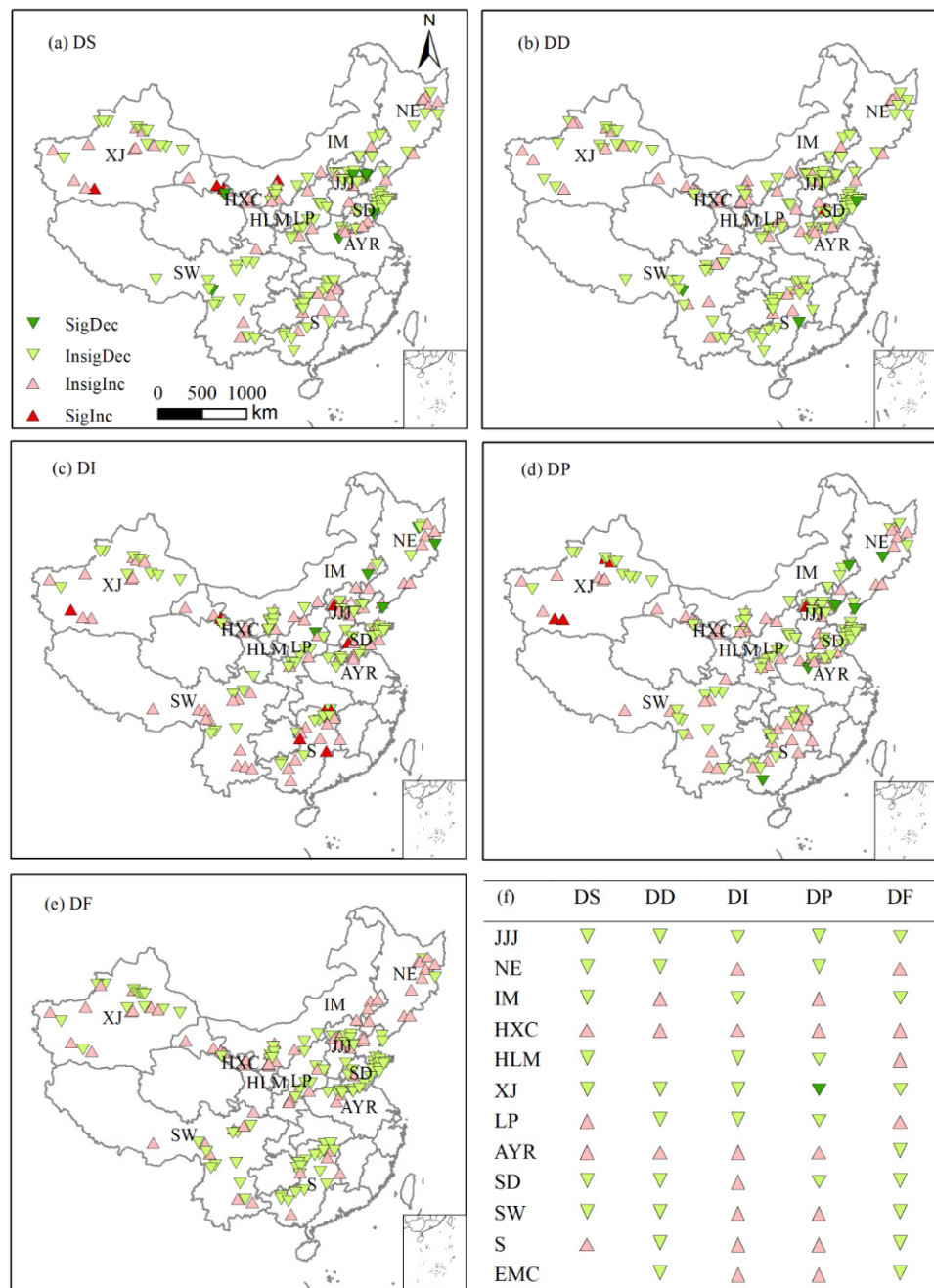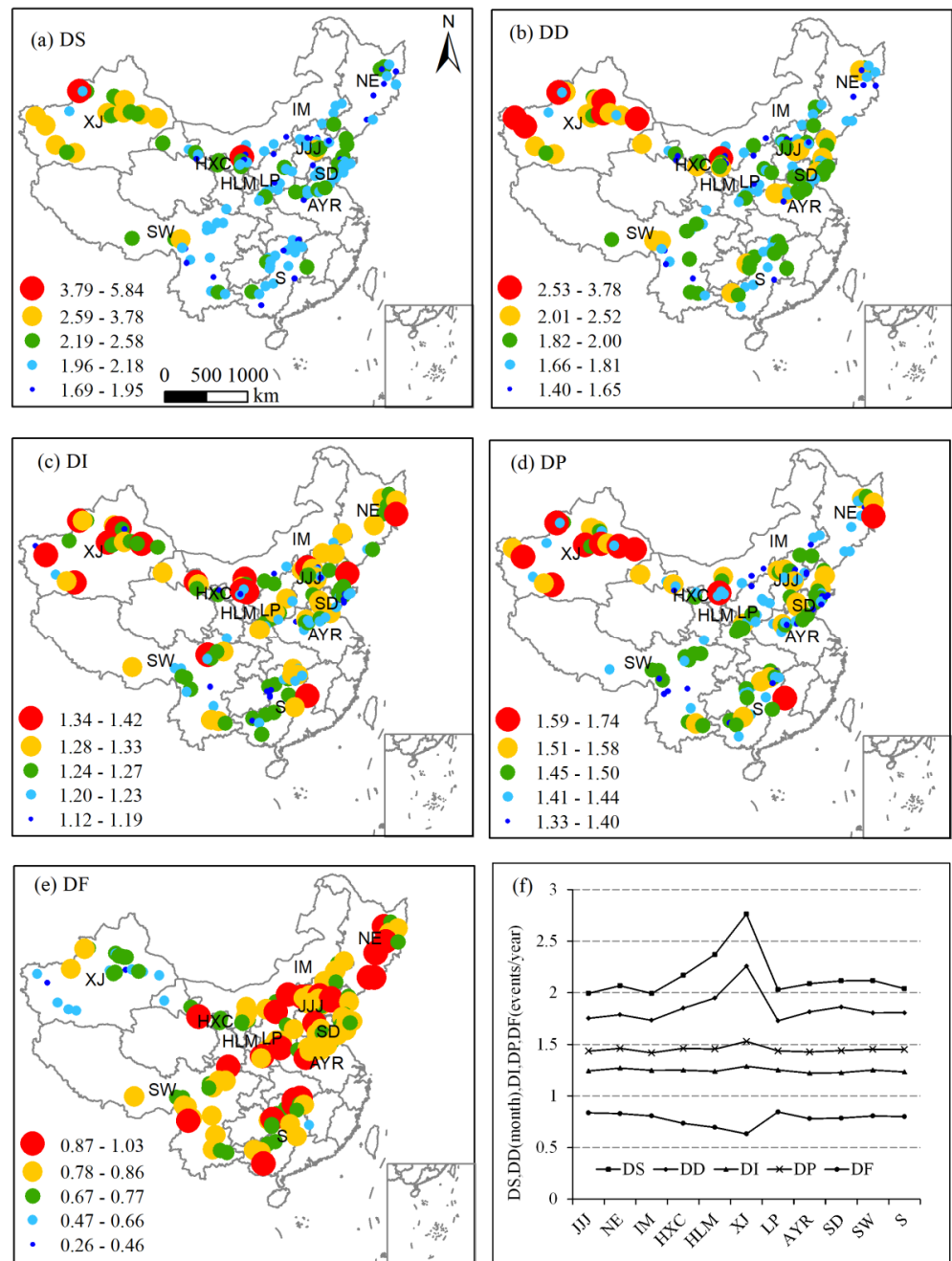**Figure 5.** Spatial patterns of drought severity (DS), drought duration (DD), drought intensity (DI), drought peak (DP), and drought frequency (DF) of the drought events identified by the SPEI1 in the wine regions of China from 1981–2015.

Table 3. Three levels of drought frequency of the drought events identified by the SPEI1 in the wine regions of China from 1981 to 2015.

Region	Number of Drought Events	Moderate Drought Frequency (%)	Severe Drought Frequency (%)	Extreme Drought Frequency (%)
JJJ	29	72.4%	27.6%	0
NE	28	57.1%	42.9%	0
IM	27	55.6%	40.7%	3.7%
HLM	30	70.0%	26.7%	3.3%
HXC	28	75.0%	21.4%	3.6%
XJ	26	57.7%	30.8%	11.5%
LP	29	62.1%	34.5%	3.5%
AYR	28	71.4%	28.6%	0
SD	27	74.1%	25.9%	0
SW	27	74.1%	25.9%	0
S	26	65.4%	30.8%	3.9%
EMC	29	55.2%	41.4%	3.5%

The drought characteristics were mutually influential; for most short-DD events, a higher DP was accompanied by a higher DI. For example, the events that occurred in July 2000 in HLM and from May–June in 2001, and in April 1997 in XJ were characterized by DP values higher than 2.00 and DI values higher than 1.50. For some cases, a high DP value did not follow a high DI value, mostly due to the long DD value; this situation was observed for the events such as May-September 1999 in NE and May-September 1997 in LP, during which the DPs were higher than 2.00 and the DIs were lower than 1.50 (Figure S1). Based on the severities of drought events, the five most serious drought events (D1–D5) in each wine region were identified (Table S1). Most of these serious drought events were detected in the 1980s and in approximately 2000 in the analyzed wine regions. Some drought events occurred across several regions, while some were regionally specific. The most serious drought events identified in JJJ and NE occurred in 1999, and those in XJ and S occurred in 1985. AYR and SD experienced the most serious drought events in 1981; in the same year, some other serious drought events occurred in JJJ and S. LP underwent the most serious drought event in 1997, while some serious drought events occurred at this time in JJJ, AYR, and SD. IM suffered its most serious drought in 2001, and many other regions also experienced serious drought events in this year, such as HLM, XJ, LP, JJJ, HCX, AYR, and NE.

3.3. Wetness Characteristics

The wetness trend characteristics in the wine regions of China are shown in Figure 6. Regional and site-specific wetness trend characteristics were observed, similar to the characteristics of the drought trends. The WS trend was consistent with the WD trend in most wine regions. NE and S showed increasing WS trends and decreasing WD trends, while AYR and SW showed increasing WS and WD trends. In other regions, these two wet characteristics both decreased. The WI trend was consistent with the WP trend in most wine regions in addition to JJJ, IM, and AYR. The NE, HLM, LP, SW, S, and the EMC experienced increasing WI and WP trends, while HCX, XJ, and SD experienced decreasing WI and WP trends. In JJJ and IM, the WI increased and the WP decreased, while AYR showed the opposite characteristics. An increasing WF trend was found in the EMC and in most wine regions except LP.

Figure 6. The trends of wet severity (WS), wet duration (WD), wet intensity (WI), wet peak (WP), and wet frequency (WF) of the wet events identified by the SPEI1 in the wine regions of China from 1981–2015. SigDec, InsigDec, InsigInc, and SigInc represent significant decrease, insignificant decrease, insignificant increase, and significant increase trends, respectively.

Figure 7 shows the spatial distribution of the wetness characteristics obtained in the wine regions of China. WS and WD exhibited similar spatial patterns. XJ was characterized by higher WS and WD values and lower WF values, indicating the occurrence of fewer but more serious wet events in this region. In contrast, HXC and HLM suffered from higher WF values but had relatively short WDs and lower WSs compared to XJ. The wet characteristics showed not only regional features but also site-specific features. More differences were

found in the WI and WP trends among stations, while fewer differences among regions were observed.
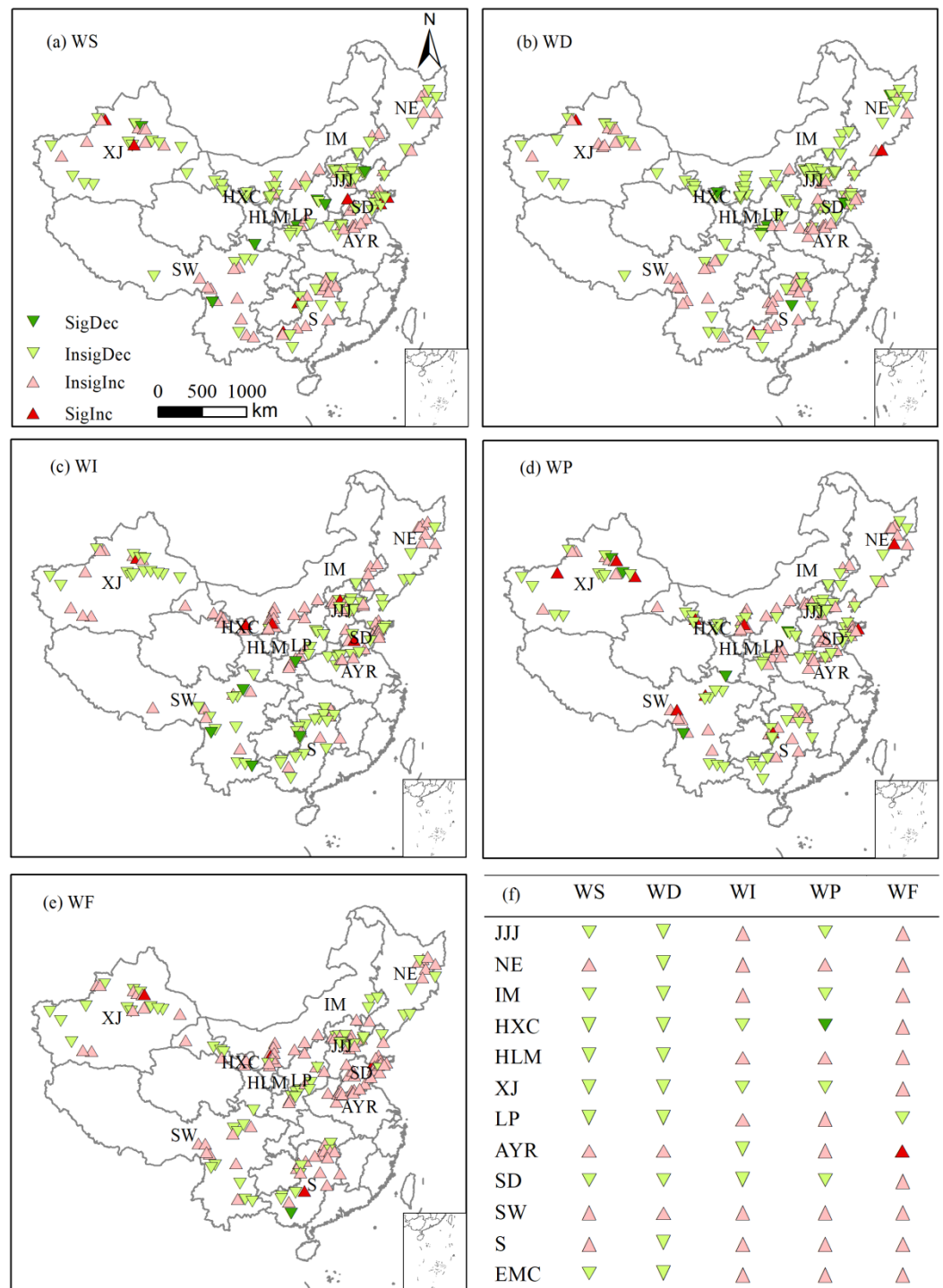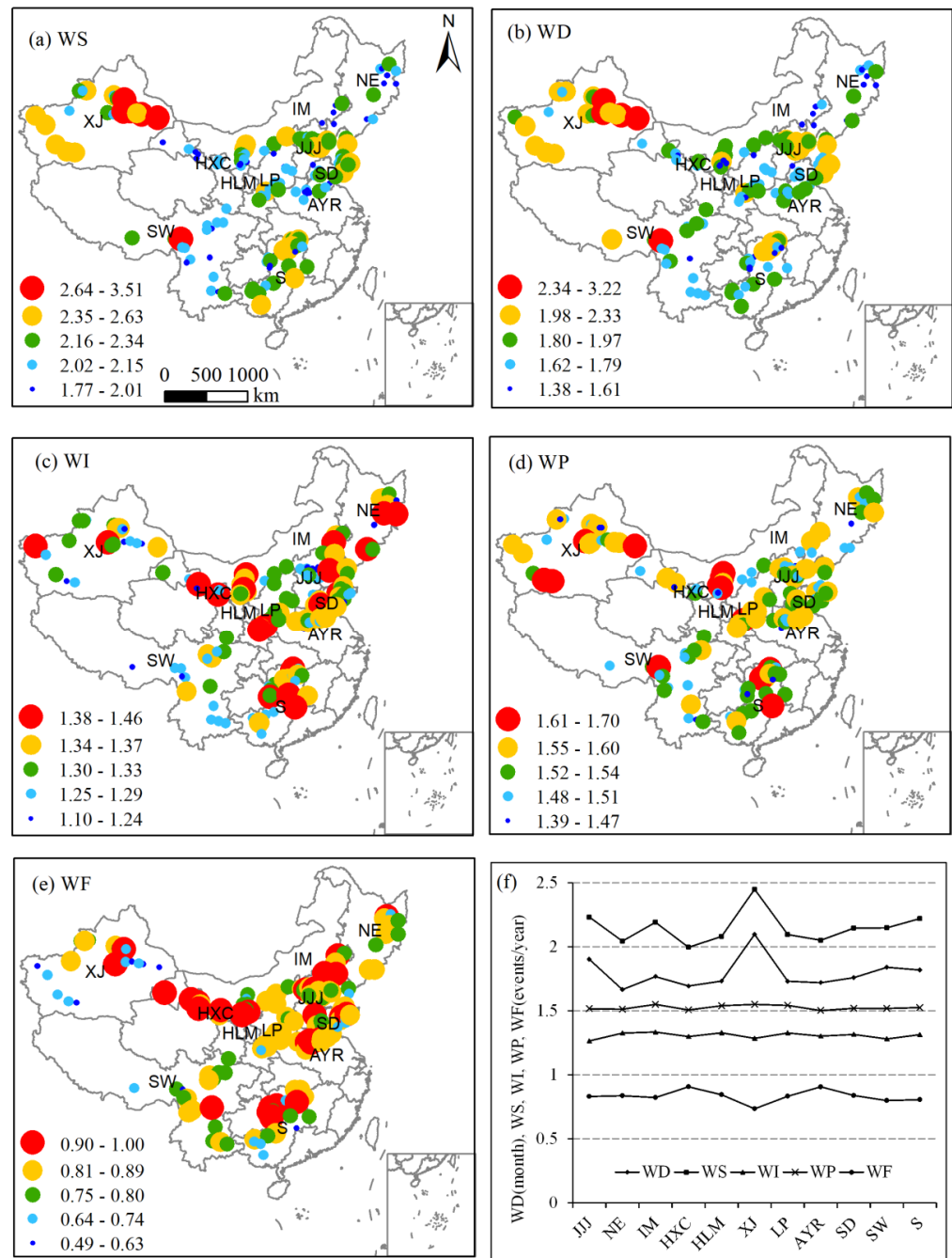

Figure 7. Spatial patterns of wet severity (WS), wet duration (WD), wet intensity (WI), wet peak (WP), and wet frequency (WF) of the wet events identified by the SPEI1 in the wine regions of China from 1981–2015.

Three levels of wetness frequencies in the analyzed wine regions are listed in Table 4. The wet events occurred most in IM and less in XJ and S. Comparing the frequencies of wet events at different levels, wet events occurred with the following frequency rank in each wine region and in the EMC: moderately wet > severely wet > extreme wet events. Extremely wet events were identified in the EMC and in all wine regions except AYR. The frequency of extremely wet events was 16.0% in XJ, which was higher than those in other regions. The frequencies of extremely wet and severely wet conditions were quite high in

HLM, HXC, and LP, at 48.28%, 46.67% and 45.16%, respectively, and were lowest in AYR, at 25%.

Table 4. Three levels of wetness frequencies of the wet events identified by the SPEI1 in the wine regions of China from 1981 to 2015.

Region	Number of Wet Events	Moderate Wet Frequency (%)	Severe Wet Frequency (%)	Extreme Wet Frequency (%)
JJJ	30	60.0%	36.7%	3.3%
NE	27	59.3%	33.3%	7.4%
IM	33	63.6%	30.3%	6.1%
HCX	30	53.3%	40.0%	6.7%
HLM	29	51.7%	34.5%	13.8%
XJ	25	64.0%	20.0%	16.0%
LP	31	54.8%	38.7%	6.5%
AYR	32	75.0%	25.0%	0
SD	28	57.1%	39.3%	3.6%
SW	29	55.2%	41.4%	3.5%
S	25	64.0%	28.0%	8.0%
EMC	26	76.9%	19.2%	3.9%

The wet characteristics are mutually influential; for most short-WD events, higher WPs are accompanied by higher WIs, as observed for the events of May 1997 in IM, April 2007 in HCX and May 2009 in LP. For some events, a higher WP did not follow a higher WI, mostly due to long WDs, as observed for the events of June-July 2013 in HLM and April-September 2003 in AYR (Figure S2). Based on the severity of wet events, the five most serious wet events (W1–W5) in each wine region were identified (Table S2). These events occurred mostly before 2000 in JJJ, NE, IM, XJ, HCX, HLM, and LP, after 2000 in AYR, and in approximately 2000 in SW and S. The most serious wet events were identified in JJJ, IM, and XJ in 1998, and some serious wet events were also identified in NE and SW in this year. HLM, SW, and S experienced the most serious wet events in 2002, and a serious wet event also occurred in HCX in this year. AYR and SD exhibited the most serious wet events in 2003; meanwhile, a serious wet event was identified in LP.

3.4. Periodicities of the SPEI

The wavelet power spectra of the SPEI6-Sep in the wine regions of China are given in Figure 8. In general, the periodicities of the SPEI varied within the range of 2–6 years. Considerable differences were also detected in the power patterns among the wine regions. JJJ and NE shared similar wavelet power spectrum patterns in which 3–5-year periodicities were identified in the 1990s and later 2000s. A significant 2-year periodicity starting approximately 2011, a 5–7-year periodicity before 2000 and an 8–10-year periodicity after 2000 were identified in IM. HCX, HLM, XJ, and LP showed similar wavelet power spectrum patterns with significant 4–6-year periodicities in the 1980s and 2–3-year periodicities in the 1990s. In the 2000s, 3–5-year periodicities were identified in all these regions except XJ. AYR and SD exhibited differences and similarities in their wavelet spectra, with a significant 4–6-year periodicity in the 2000s in AYR and a significant 2–3-year periodicity in approximately 1991 in SD. Moreover, 5–7-year periodicities in the 1980s and 2-year periodicities in the late 1990s were identified in these two regions. A 2–3-year periodicity was identified in the 1990s and late 2000s in SW. A 5–7-year periodicity was identified around the 1990s followed by a decreasing periodicity in S. For the EMC, a 4–6-year periodicity and significant power pattern were identified around the 2000s. The wavelet power spectrum patterns in these regions were consistent with most drought and wet events that occurred from 1981 to 2015. The small periodicities could explain the intense drought and wet events, while the larger periodicities could explain the occurrence of scattered events in certain periods.
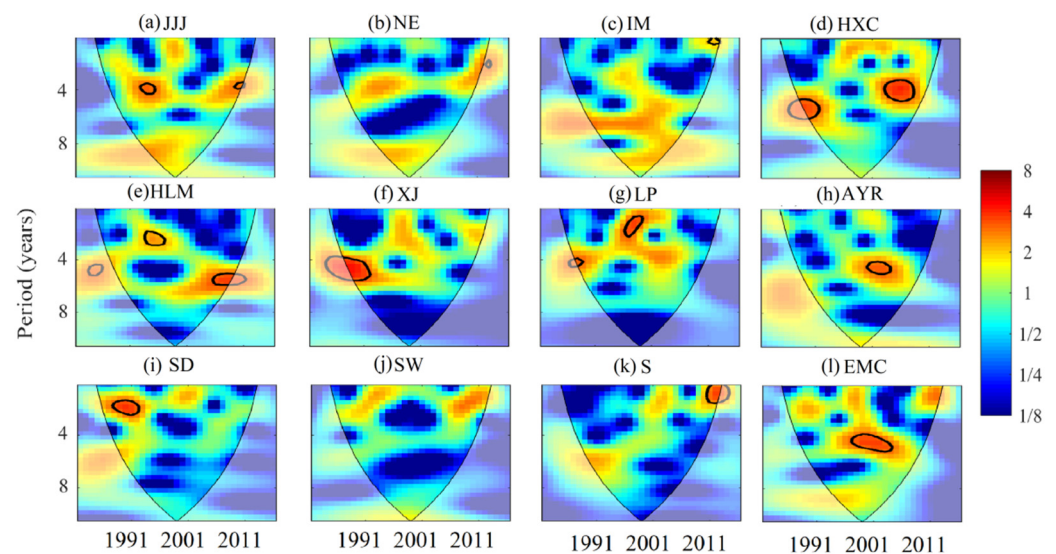
Figure 8. The wavelet spectra of the SPEI6-Sep in the wine regions of China from 1981–2015 are shown. The colors from blue to red indicate the increasing wavelet power. The thin solid lines demarcate the cones of influence, and the thick solid lines show the 95% confidence levels.

3.5. Relations between the SPEI and Climatic Factors

Observations of climate change have indicated that atmospheric responses to external forcings can last for a long time. In this study, the correlation coefficients between SPEI6-Sep and large-scale climate factors (SOI, Niño 3.4 and IOD) in the wine regions of China were calculated considering the effect of lag times and the results are shown in Table 5. The lag effects of climate factors on the SPEI6-Sep were obvious, and the dryness/wetness variability was sensitive to climate factors since the correlation coefficients were significant (Table 5). The response times of the EMC to SOI, Niño 3.4, and IOD were 11, 8, and 11 months, respectively. The lag times with which these climate factors influenced the SPEI6-Sep of each wine region were scattered. The SOI had significant negative correlations with the SPEI6-Sep in NE, IM, HXC, XJ, and S with lag times of 5, 7, 9, 9, and 11 months, respectively, and a weak correlation with SPEI6-Sep in SW. In other regions, the SOI had a positive correlation with SPEI6-Sep with a 1-month lag time, and significant correlations were also found in HLM and LP. Niño 3.4 and SPEI6-Sep had significant positive correlations in NE, IM, HCX, XJ, and S with lag times of 5–10 months. Moreover, negative correlations with lag times of approximately 0–4 months were found in other regions, and significant correlations were found in SD and LP. SW showed a weak correlation between Niño 3.4 and the SPEI6-Sep. The IOD was significantly positively correlated with the SPEI6-Sep in JJJ, NE, HXC, AYR, SD, SW, and EMC, with lag times of 8–12 months, and was weakly correlated with the SPEI6-Sep in S. In other regions, the IOD had a significant negative correlation with the SPEI6-Sep with lag times of 4–6 months, except in LP, where the lag time was 0 months.

Table 5. The correlation coefficients between the SPEI6-Sep and large-scale climatic factors with lag times from 0 to 12 months in the wine regions of China.

Index	Region	Lag Time (Months)												
		0	12	11	10	9	8	7	6	5	4	3	2	1
SOI	JJJ	0.15	−0.11	0.04	−0.07	0.05	−0.01	0.02	0.13	−0.11	0.02	0.11	0.18	_0.26_
	NE	0.05	−0.28	−0.29	−0.37	−0.31	−0.32	**_−0.41_**	−0.31	−0.26	−0.07	0.19	0.14	0.12
	IM	−0.24	−0.34	−0.36	−0.33	−0.27	−0.31	−0.19	−0.35	**_−0.46_**	−0.18	−0.23	−0.06	−0.05
	HXC	0.15	−0.43	−0.51	−0.39	**_−0.54_**	−0.48	−0.42	−0.36	−0.28	0.03	−0.03	−0.07	0.11
	HLM	0.30	0.00	0.01	0.18	−0.11	−0.13	0.09	0.12	0.12	0.27	0.13	0.23	**_0.32_**
	XJ	0.20	−0.46	−0.45	−0.39	**_−0.58_**	−0.53	−0.46	−0.42	−0.34	0.09	0.14	0.16	0.19
	LP	0.51	−0.04	−0.11	−0.11	−0.18	−0.19	−0.23	−0.14	0.25	0.48	0.24	0.43	**_0.52_**
	AYR	0.18	−0.06	−0.06	−0.02	0.04	−0.13	0.06	0.09	0.10	0.06	−0.12	0.03	_0.26_
	SD	0.17	0.08	−0.05	0.00	0.01	−0.06	−0.04	0.20	0.02	0.06	0.07	0.21	_0.27_
	SW	−0.12	−0.09	−0.06	0.06	0.00	−0.04	0.12	−0.05	−0.11	−0.09	_−0.14_	0.02	0.07
	S	−0.20	−0.24	**_−0.40_**	−0.16	−0.19	−0.17	−0.11	−0.25	−0.32	−0.15	−0.18	−0.23	−0.23
	EMC	0.11	−0.27	**_−0.40_**	−0.22	−0.25	−0.31	−0.19	−0.17	−0.26	0.02	−0.01	0.12	0.23
Niño 3.4	JJJ	−0.08	0.10	0.08	0.06	0.02	0.07	0.05	−0.01	−0.11	_−0.15_	−0.13	−0.02	−0.02
	NE	0.01	0.31	0.31	**_0.33_**	0.30	0.32	0.32	0.30	0.24	0.17	0.09	0.05	0.07
	IM	0.13	0.24	0.22	0.20	0.21	**_0.30_**	**_0.30_**	0.27	0.24	0.22	0.09	0.14	0.16
	HXC	−0.24	0.43	0.43	0.42	0.46	**_0.48_**	**_0.48_**	0.46	0.35	0.20	0.05	−0.19	−0.22
	HLM	−0.27	0.02	−0.02	−0.01	−0.04	0.01	0.04	−0.01	−0.12	−0.24	_−0.28_	−0.20	−0.24
	XJ	−0.24	0.55	0.55	0.59	0.59	0.61	0.60	**_0.62_**	0.52	0.28	0.05	−0.12	−0.23
	LP	−0.48	0.30	0.24	0.25	0.25	0.23	0.21	0.19	−0.02	−0.19	−0.37	−0.47	**_−0.50_**
	AYR	−0.21	0.03	0.05	0.01	0.03	0.05	0.00	−0.08	−0.12	−0.17	_−0.22_	−0.14	−0.17
	SD	**_−0.30_**	0.10	0.08	0.07	0.04	0.08	0.03	−0.03	−0.09	−0.21	−0.25	−0.17	−0.23
	SW	−0.05	0.01	−0.02	−0.01	−0.02	0.03	0.01	−0.02	−0.03	_−0.11_	_−0.11_	−0.01	0.00
	S	0.15	0.24	0.24	0.26	0.25	0.27	0.25	0.29	**_0.34_**	0.25	0.21	0.14	0.16
	EMC	−0.20	0.35	0.32	0.34	0.31	**_0.36_**	0.32	0.28	0.18	−0.01	−0.12	−0.10	−0.13
IOD	JJJ	0.00	0.38	0.30	0.13	0.07	**_0.43_**	0.04	0.14	−0.06	−0.04	0.00	−0.03	0.10
	NE	0.01	0.23	0.28	0.25	0.21	**_0.36_**	−0.14	−0.18	0.05	0.05	−0.06	−0.08	0.06
	IM	0.11	0.18	0.15	0.14	0.12	0.24	−0.11	_−0.25_	0.00	0.02	−0.06	0.15	0.08
	HXC	−0.15	0.21	**_0.38_**	0.35	0.27	0.07	−0.11	_−0.38_	−0.23	0.03	−0.04	0.01	−0.17
	HLM	−0.11	0.42	0.41	0.21	0.22	0.00	−0.12	−0.10	−0.37	**_−0.56_**	−0.41	−0.11	−0.13
	XJ	−0.32	0.29	0.32	0.35	0.38	0.00	−0.22	**_−0.41_**	−0.27	−0.11	−0.15	−0.19	−0.33
	LP	**_−0.42_**	0.28	0.39	0.23	0.14	0.06	−0.16	−0.17	−0.16	−0.24	−0.15	−0.16	−0.21
	AYR	−0.11	**_0.31_**	0.28	0.11	0.05	−0.09	−0.13	0.09	0.06	0.09	−0.03	−0.02	0.00
	SD	−0.19	0.27	0.21	0.09	0.02	**_0.35_**	−0.08	0.13	−0.02	0.02	0.02	−0.05	0.02
	SW	−0.01	0.11	−0.02	0.06	0.12	0.13	**_0.36_**	0.30	0.15	0.00	0.04	−0.05	−0.06
	S	0.13	0.02	0.12	0.13	0.14	0.07	0.11	−0.10	−0.14	0.00	_0.16_	0.15	0.14
	EMC	−0.11	0.39	**_0.43_**	0.29	0.24	0.35	0.01	−0.05	−0.14	−0.06	0.02	0.00	0.04

T statistics were used to test the correlations between SPEI6-Sep and SOI, Niño 3.4 and IOD with different lag times; the critical correlation coefficients were 0.283, 0.334 and 0.430 at significance levels of 10%, 5%, and 1%, respectively. The italic, underlined and bold values indicate the highest significant correlation that was significant at the 10% level.

According to the correlation and lag time analyses, the relationships between the SPEI6-Sep and climatic indices with the highest correlations in the wine regions were explored using the bivariate wavelet coherence method, taking advantage of scale specificity and localization (Figures 9–11). The relationships between the SPEI6-Sep and SOI in the wine regions of China are illustrated in Figure 9. The SOI negatively affected the SPEI6-Sep in NE, IM, HXC, XJ, S, and EMC on different time scales and temporal domains. For example, an anti-phase coherence pattern was recognized in a 2–6-year band before 2011 in HXC and in a 3–6-year band from 1981–2015 in XJ. The correlation was highest in XJ, as evidenced by a remarkable coherence pattern. This relationship indicated that a higher SOI value led to a lower SPEI6-Sep value in these regions, corresponding to the occurrence of serious drought events. On the other hand, significant positive correlations between the SPEI6-Sep and SOI could be recognized in JJJ, HLM, LP, AYR, and SD on different time scales and temporal domains. For example, significant in-phase coherence patterns were identified in a 3–7-year band before 2000 in HLM and in a 2–7-year band before 2010 in LP. These relationships indicate that a higher SOI value results in a higher SPEI6-Sep value in these regions, resulting in the occurrence of serious wet events.
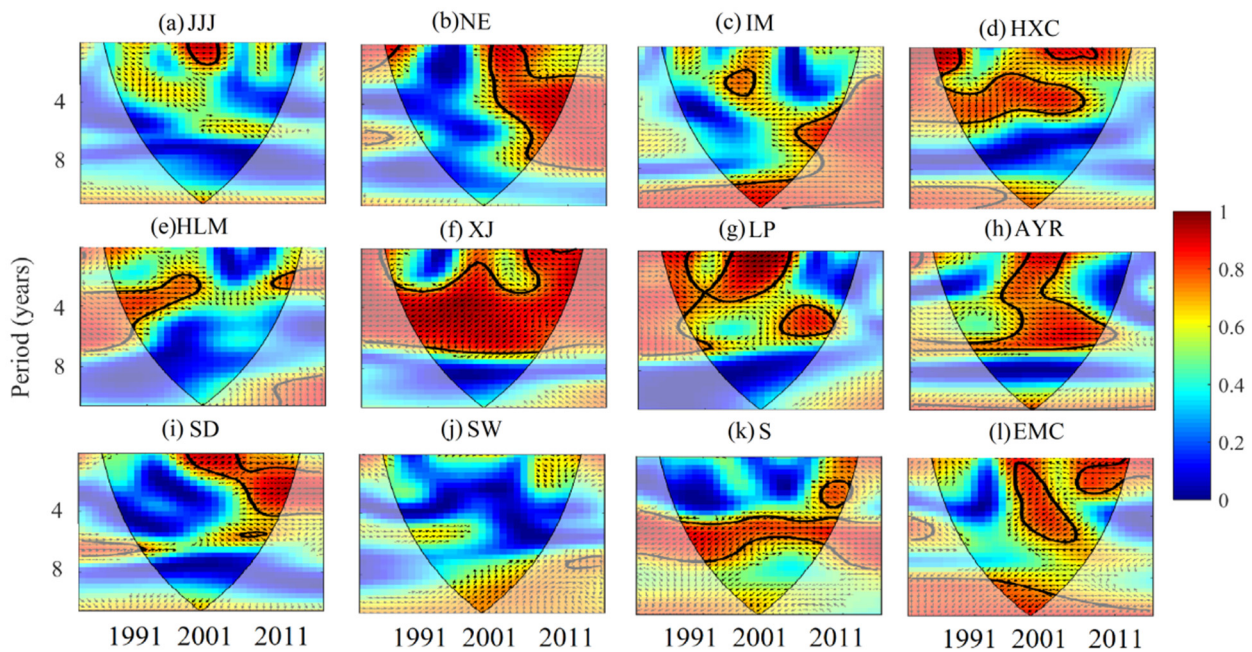
Figure 9. The bivariate wavelet coherency between the SPEI6-Sep and SOI in the wine regions of China from 1981–2015. The colors from blue to red indicate increasing coherence. The phase relationships between the SPEI6-Sep and SOI are denoted by arrows (in-phase arrows point right and anti-phase arrows point left); the thin solid lines demarcate the cones of influence, and the thick solid lines show the 95% confidence levels.

Figure 10. The bivariate wavelet coherency between the SPEI6-Sep and Niño 3.4 in the wine regions of China from 1981–2015. The colors from blue to red indicate increasing coherence. The phase relationships between the SPEI6-Sep and Niño 3.4 are denoted by arrows (in-phase arrows point right and anti-phase arrows point left); the thin, solid lines demarcate the cones of influence, and the thick solid lines show the 95% confidence levels.
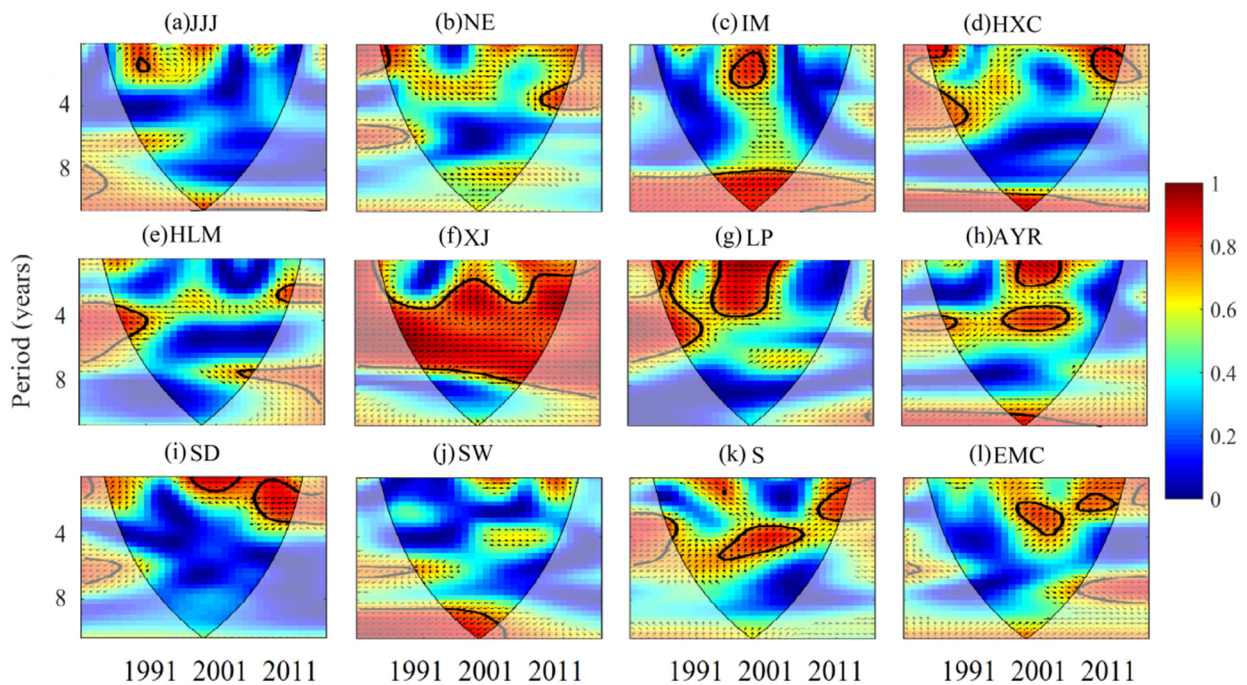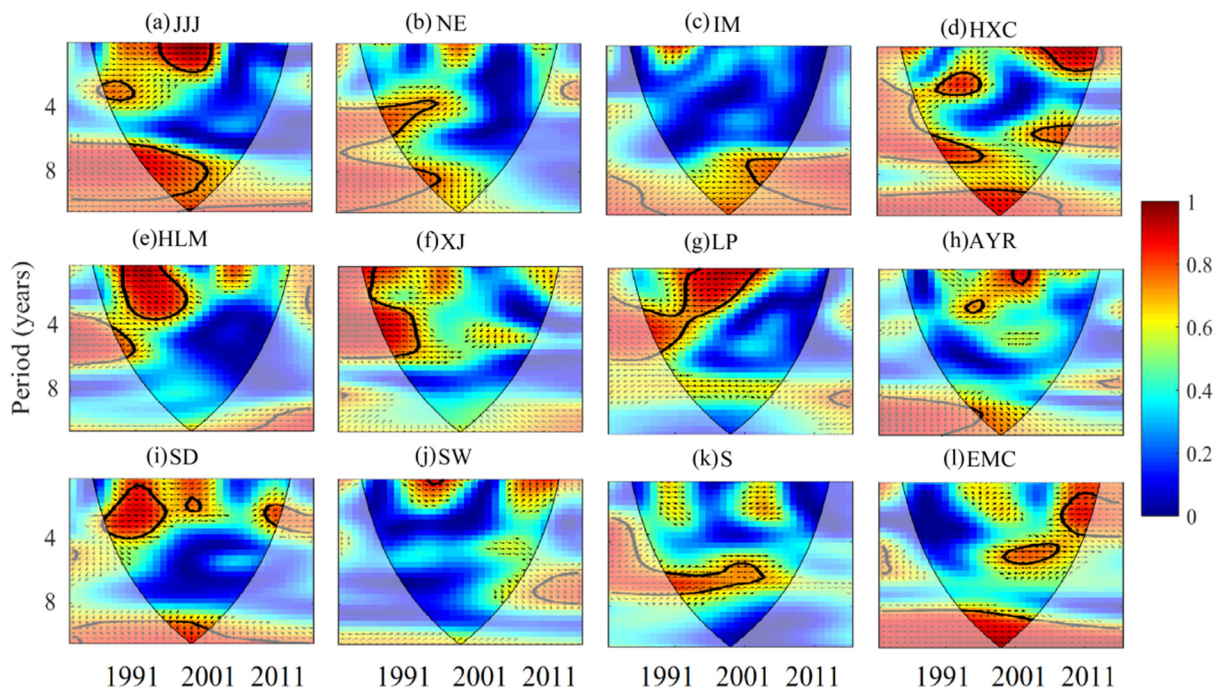
Figure 11. The bivariate wavelet coherency determined between the SPEI6-Sep and IOD in the wine regions of China from 1981–2015. The colors from blue to red indicate increasing coherence. The phase relationships between SPEI6-Sep and IOD are denoted by arrows (in-phase arrows point right and anti-phase arrows point left); thin solid lines demarcate the cones of influence, and thick solid lines show the 95% confidence levels.

Niño 3.4 positively affected the SPEI6-Sep in NE, IM, HXC, XJ, S, and EMC and negatively affected the index in other regions on different time scales and temporal domains; these results are opposite to the effects of the SOI (Figure 10). However, the correlation pattern between Niño 3.4 and the SPEI6-Sep shared similarities with that between SOI and SPEI6-Sep in the analyzed wine regions. Significant patterns appeared at similar locations in the same region, although the scales and temporal amplitudes sometimes had few differences. For example, in XJ, the 3–6-year bands identified during the whole study period were found to be under the influence of both the SOI and Niño 3.4. In NE, the effect of Niño 3.4 on the SPEI6-Sep was higher before 1990 with a 2–3-year band and an approximately 6-year band, similar to the effect the SOI had on SPEI6-Sep before 1990. Niño 3.4 also exhibited an obvious influence on the SPEI6-Sep in NE since 2005 in a 2–4-year band in which the significant band shrank compared to the band of the SOI and SPEI6-Sep relation since 2000. Compared to the correlation pattern between the SOI and SPEI-Sep in the EMC, the significant patterns of Niño 3.4 and SPEI-Sep shrank at small scales after 1995, and a new, large-scale significant pattern appeared after 2005.

The IOD significantly positively affected the SPEI6-Sep in JJJ, NE, HXC, AYR, SD, S, and EMC on different time scales and temporal domains (Figure 11). For example, in JJJ, a strong positive coherence between the IOD and SPEI6-Sep could be observed in a 6–9-year band before 2001 and in a 2–4-year band during 1985–2001. In HXC, this coherence could be observed in a 3–7-year band before 1998 and a 2–3-year band from 2006–2013. On the other hand, significant negative correlations between the SPEI6-Sep variation and IOD could be recognized in the IM, HLM, XJ, and LP on different time scales and temporal domains. Strong negative coherence between the IOD and SPEI6-Sep could be observed within a large time scale (8–10 years) in IM during the whole study period, and significant coherence was detected from 1980–1990 and from 2003–2015. HLM, XJ, and LP shared similar coherence patterns with strong negative correlations between the IOD and SPEI6-Sep in a 2–6-year band before 2001. The IOD showed a weak influence on the SPEI6-Sep in SW, as evidenced

by a weak coherence pattern. A significant coherence in the 6–8-year band was detected for the IOD after 2010 in this region, and this result might be affected by potential edge effects.

4. Discussion

4.1. Impacts of the Time Scale and Evapotranspiration on the SPEI

The SPEI is one of the most common recently used indices for monitoring dryness and wetness, and this index can be applied on a variety of time scales (such as 1, 3, 6, 12, or 24 months), allowing the SPEI to be used to analyze the impacts of dryness and wetness on various types of hydrologic conditions. Durations of weeks or months can be used to apply this index to agricultural research, while longer durations spanning years can be used to apply this index to water supply and water management research [43]. We used the SPEI1 and SPEI6-Sep to reflect the evolution and characteristics of dryness/wetness in the wine regions of China. Various studies have used the SPEI at different time scales and in certain months to indicate the dryness and wetness conditions associated with agricultural crops [44–46]. The SPEI6-Oct was used to analyze the spatiotemporal distribution and variation characteristics of summer maize drought on the North China Plain [44]. The SPEI3-Oct, SPEI3-Jan, SPEI3-Jun, and SPEI12-Jun were used to indicate the strength of drought affecting winter wheat in Henan Province at different growth stages and throughout the whole growth stage [46]. The SPEI3-May, SPEI3-July, SPEI3-Sep, and SPEI6-Sep were used to denote temporal and spatial maize drought characteristics during different growth stages and throughout the whole growth stage in Yunnan Province [45]. However, in these studies, the SPEI output the reference evapotranspiration, which did not correspond exactly to the evapotranspiration of the studied crops. Crop evapotranspiration differs distinctly from reference evapotranspiration, as the ground cover, canopy properties, and aerodynamic resistance of crops are different from those of grasses [25]. Evapotranspiration has been confirmed to play a critical role in the SPEI; it can aggravate the drought degree in areas with reduced precipitation and lead to a change from a wet climate to a dry climate in areas with slightly increased precipitation [47,48]. In addition, the roles of different climatic variables in determining drought evolution varied. This research did not focus on which climatic factors control the dryness and wetness in the different sub-regions. We will further consider the impact of different regional climate factors on drought/wet assessment in future studies.

A calculation method used to obtain evapotranspiration from a specific crop surface by multiplying the reference evapotranspiration by a crop coefficient, which integrates the differences in evaporation and transpiration between field crops and the reference grass surface, has been suggested [19]. Due to differences in albedo, crop height, aerodynamic properties, and leaf and stomatal properties, different crops have different crop coefficients. The changing characteristics of the same crop over the growing season also affect the crop coefficient. In our research, we calculated the SPEI using the studied crop (grapevine) coefficient to calculate the evapotranspiration, thus improving the reliability of the SPEI characterizing wine regions.

4.2. Variations in the SPEI and Dryness/Wetness Characteristics

The variations in the SPEI and dryness/wetness characteristics in the wine regions of China were found to be region-specific, site-specific, and complicated; these results were consistent with the drought situation in China as reported by Yao et al. [9]. From the relatively detailed comparison, different conclusions have been obtained in publications concerning drought evolution in China, and most research has indicated general drought relief over the last several decades in the EMC [9,49,50]. The general increases in the SPEI1 and SPEI6-Sep calculated in the EMC in this study were consistent with these results. However, the SPEI trends performed differently among the different wine regions. Most regions showed increasing trends, and only a few regions showed decreasing trends. XJ ranked first with a grapevine cultivation area of 36,700 ha, followed by HLM with 34,000 ha. HXC ranked third, with grapevines covering an area of 20,500 ha. These top three regions

accounted for approximately 55% of the total grapevine cultivation area in China [4]. XJ and HLM showed increasing SPEI trends, while HXC showed a decreasing SPEI trend. This was consistent with reports that XJ was dominated by a wetting trend and HXC was dominated by a dry trend from 1966 to 2015 [18]. The SPEI was not only regionally specific but was also site-specific; within a wine region, some sites showed increasing trends, while others showed decreasing or no trends. The wine regions in China were located in mountain, plain, hilly, or basin areas at different elevations; for example, the standard deviation of SW reached nearly 580 m, and this region is situated in the Hengduan Mountains. The geographical and topographic differences of the studied regions resulted in distinct differences in the climatic characteristics within and between wine regions [4]. Similar to the SPEI, the dryness/wetness characteristics were region- and site-specific with similar geographical and topographic drivers. In other words, the SPEI and dryness/wetness characteristics were not only regional but were also site-specific, and comparing the water resource allocation and utilization between and within regions is thus challenging.

XJ presented drought and wetness events with higher average severities and longer durations as well as the highest extreme drought and wetness event frequencies. It was easy to understand that the serious drought situation in XJ can be attributed to its arid and semiarid climate. When analyzing serious wet events, one should know that the SPEI is a standardized index that indicates the probability of the occurrence of an observed water surplus or deficiency in the studied region. The dryness and wetness conditions were determined relative to the historical averages rather than using the absolute difference between precipitation and evapotranspiration at a particular location. Moreover, the arid areas also experience floods due to the uneven distribution of precipitation, and rainstorms and floods reportedly occurred more than 2000 times between 1949 and 1997 in XJ [4]. XJ is known as the largest wine region as well as an excessively water-stressed area in China; the grapevine in this region relies on irrigation. The harvests in lands that experience rain and irrigation in a drought year could be reduced by 40% and 30%, respectively, due to the scarcity of water resources [51]. Thus, water resource management and allocation for grapevines in XJ is absolutely necessary, and appropriate water usage plans should be prioritized and developed in this region.

4.3. Influence of ENSO and the IOD on Dryness/Wetness

Many serious dry and wet events were identified in 2001 and 1998, respectively, in the analyzed wine regions. Another extremely desiccative year was identified in 2001 in China after the continuous excessive drought events that occurred in 1999 and 2000. The drought-affected area reached 3846×10^4 hm^2, the average grain yield decreased by approximately 5%, and the direct economic losses exceeded 100 billion Yuan. The grape yield in 2001 in China was the lowest since 1996 [52], which might have been due to the water resource shortage in China as a whole. The drought that occurred in 2001 in China was speculated to be a consequence of anomalous atmospheric circulation over Eurasia [53]. In 1998, a mega-flood swept through China's major river basins, including the Yangtze, Songhua, Nen, Min, and Pearl Rivers, and these floods affected 186 million people, caused 4150 deaths, and led to a total economic loss of 436 billion Yuan [54]. The disastrous floods that occurred in the entire Yangtze River basin in 1998 were a direct result of unusually high precipitation (670 mm) due to a strong El Niño event [11].

The SPEI periodicities identified in the wine regions of China were mainly constrained within 2–6-year bands, and a common significant 4–6-year periodical oscillation could be detected over the wine regions, consistent with the ENSO periodicity, which varied between 2 and 7 years with an average of approximately 4 years [55,56]. Thus, studying the links between large-scale climate patterns and SPEI variations is helpful for understanding the formation mechanisms of dry and wet events. As supposed, the climatic factors ENSO and the IOD significantly influenced the SPEI in the wine regions of China, possibly because distinctive regional and seasonal precipitation patterns were identified in China under the impacts of ENSO and the IOD [21,57,58]. The impact of ENSO on precipitation

varied regionally; the summer, autumn, and winter precipitation and annual precipitation decreased in the northern part of eastern China, while the autumn precipitation in the southern part of China and the winter precipitation in southeastern China apparently increased in the El Niño-developing year [21]. The rainfall over China was remotely influenced by different IOD phases via changes in the intensity of the southern Asian High and western North Pacific summer monsoon [22,58,59]. During positive IOD events, the associated low-level anomalous anticyclones that develop over the Bay of Bengal and the South China Sea strengthen the south-westerlies, thus leading to an increased moisture flux that gives rise to anomalously high precipitation over southern China [58]. When ENSO co-occurs with the IOD, the influences exerted by one phenomenon on precipitation in different regions of China might be enhanced or weakened by other phenomena [59], and the positive phase of the combined ENSO and IOD events might result in increased autumn rainfall over southern China [60]. In general, the responses of the SPEI to climate indices differed regionally, with some regions simultaneously affected by a given climate index and the influences of that climate index modulated by another climate index.

The responses of the SPEI to the Niño 3.4, SOI, and IOD varied among different stages, and the lag effects associated with climatic factors were obvious. ENSO and drought are closely correlated with a certain time lag, as has been determined in many regions of the world [60]. The lag effects of the Niño 3.4, SOI, and IOD indices on the SPEI were similar to the results reported by Chen et al. [11], who found that the main dryness/wetness patterns were positively correlated with Niño 3.4 and the IOD and negatively correlated with the SOI with lag times of 8–12 months [11]. In addition, the lag effects of the IOD and Niño 3.4 on the SPEI were found to be consistent with the findings that an increased rainfall amount occurs after the occurrence of positive IOD a year before [22] and that precipitation is positively correlated with the ENSO one year ahead in the eastern part of China [61]. With the background of climate change, the results that the main climatic factors, ENSO and the IOD, affect the SPEI with a given lag time are important for the prediction and mitigation of potential risks in the wine regions of China. However, there are hundreds of atmospheric circulation factors. We only analyzed the effects of ENSO and IOD on dryness/wetness changes in this study, and there are some uncertainties.

5. Conclusions

The different time scales on which the SPEI was analyzed in the entire wine region of China showed an overall wetting trend from 1981 to 2015. The regional characteristics of the SPEI were obvious as well; most wine regions experienced wetting trends, such as the Jing-Jin-Ji, Inner Mongolia, Helan Mountain, Xinjiang, Ancient Yellow River, Shandong, and Special regions, while a few wine regions experienced drying trends, such as the Northeast, Hexi Corridor, Loess Plateau, and Southwest regions.

The dryness and wetness characteristics in the analyzed wine regions of China were found to be region-specific, site-specific, and complicated. Great dryness/wetness differences were identified among stations and regions due to differences in climatological, geographical, and topographic features between and within the studied wine regions. The Xinjiang, Helan Mountain, and Hexi Corridor regions accounted for approximately 55% of the total grapevine cultivation area in China and suffered from higher drought/wet severities and extreme drought frequencies, which aggregated the water resource allocation and risk mitigation pressures for the wine industry in these regions of China.

A common, significant 4–6-year periodical oscillation of the SPEI was observed in the wine regions of China. This was consistent with the ENSO periodicity, which varied between 2 and 7 years, with an average periodicity of approximately 4 years. The dryness/wetness characteristics in the wine regions of China were highly associated with the Southern Oscillation Index, Niño 3.4 and the Indian Ocean Dipole, with correlations of −0.40, 0.36, and 0.43 and lag times of 11, 8, and 11 months, respectively. The Southern Oscillation Index, Niño 3.4, and Indian Ocean Dipole affected the dryness/wetness conditions differently in different wine regions of China; Niño 3.4 had a positive correlation

with SPEI6-Sep in the Northeast, Inner Mongolia, Hexi corridor, Xinjiang, and Special regions as well as in the entire wine region of mainland China and a negative correlation with SPEI6-Sep in other regions; this was opposite to the effect of the SOI. The IOD had a significantly positive correlation with SPEI6-Sep in the Jing-Jin-Ji, Northeast, Hexi Corridor, Ancient Yellow River, Shandong, and Special regions as well as in the entire wine region of mainland China, while the IOD had a negative correlation with SPEI6-Sep in the other studied regions. The serious dry events that occurred in 2001 and wet events that occurred in 1998 in the analyzed wine regions might be consequences of anomalous atmospheric circulation patterns.

This study can provide a scientific basis for optimizing grape irrigation systems and alleviating the effects of drought/wet on wine grape production. However, it did not connect the drought/wet conditions to wine production directly due to the shortage of wine grape production data. In future studies, we will explore the relationship between drought/wet conditions and wine production by solving the wine grape production data problem in China.

Supplementary Materials: The following supporting information can be downloaded at: https://www.mdpi.com/article/10.3390/agronomy12040843/s1, Figure S1: Temporal patterns of drought severity (DS), drought intensity (DI), drought peak (DP), drought duration (DD) and drought frequency (DF) of the drought events identified by the SPEI1 in the wine regions of China during 1981-2015; Figure S2: Temporal patterns of wet severity (WS), wet duration (WD), wet intensity (WI), wet peak (WP) and wet frequency (WF) of the wet events identified by the SPEI1 in the wine regions during 1981-2015; Table S1: The drought duration (DD), drought peak (DP), drought severity (DS) and drought intensity (DI) of the five most severe drought events identified by SPEI1 in the wine regions of China during the period from 1981 to 2015. Drought events in each wine region are sorted out based on the drought severity from high to low. Table S2: The wet duration (WD), wet peak (WP), wet severity (WS) and wet intensity (WI) of the five most severe wet events identified by SPEI1 in the wine regions of China during the period from 1981 to 2015. Wet events in each sub-region are sorted out based on the drought severity from high to low.

Author Contributions: Conceptualization, X.Y. and B.L.; Methodology, X.Y.; Software, N.Y. and W.H.; Validation, X.Y. and N.Y.; Formal Analysis, X.Y., N.Y. and X.J.; Investigation, Y.L. and W.B.; Resources X.J. and Q.L.; Data Curation, X.Y. and X.J.; Writing—Original Draft Preparation, X.Y.; Writing—Review & Editing, X.Y., N.Y., W.H. and B.L.; Visualization, D.C.; Supervision, B.L.; Project Administration, B.L.; Funding Acquisition, X.Y. and B.L. All authors have read and agreed to the published version of the manuscript.

Institutional Review Board Statement: Not applicable.

Informed Consent Statement: Not applicable.

Data Availability Statement: Not applicable.

Conflicts of Interest: The authors declare no conflict of interest.

References

1. Griesser, M.; Weingart, G.; Schoedl-Hummel, K.; Neumann, N.; Becker, M.; Varmuza, K.; Liebner, F.; Schuhmacher, R.; Forneck, A. Severe drought stress is affecting selected primary metabolites, polyphenols, and volatile metabolites in grapevine leaves (*Vitis vinifera cv. Pinot noir*). *Plant Physiol. Biochem.* **2015**, *88*, 17–26. [CrossRef] [PubMed]
2. OIV. *State of the Vitiviniculture World Market*; OIV: Paris, France, 2016.
3. Blotevogel, S.; Schreck, E.; Laplanche, C.; Besson, P.; Saurin, N.; Audry, S.; Viers, J.; Oliva, P. Soil chemistry and meteorological conditions influence the elemental profiles of West European wines. *Food Chem.* **2019**, *298*, 125033. [CrossRef] [PubMed]
4. Wang, X.; Xie, X.; Chen, N.; Wang, H.; Li, H. Study on current status and climatic characteristics of wine regions in China. *Vitis* **2018**, *57*, 9–16. [CrossRef]
5. Du, F.; Deng, W.; Yang, M.; Wang, H.; Mao, R.; Shao, J.; Fan, J.; Chen, Y.; Fu, Y.; Li, C.; et al. Protecting grapevines from rainfall in rainy conditions reduces disease severity and enhances profitability. *Crop Prot.* **2015**, *67*, 261–268. [CrossRef]

6. Meng, J.F.; Ning, P.F.; Xu, T.F.; Zhang, Z.W. Effect of Rain-Shelter Cultivation of Vitis vinifera cv. Cabernet Gernischet on the Phenolic Profile of Berry Skins and the Incidence of Grape Diseases. *Molecules* **2012**, *18*, 381–397. [CrossRef]

7. Stagge, J.H.; Tallaksen, L.M.; Gudmundsson, L.; Van Loon, A.F.; Stahl, K. Candidate Distributions for Climatological Drought Indices (SPI and SPEI). *Int. J. Climatol.* **2015**, *35*, 4027–4040. [CrossRef]

8. Yao, N.; Li, L.; Feng, P.; Feng, H.; Liu, D.L.; Liu, Y.; Jiang, K.; Hu, X.; Li, Y. Projections of drought characteristics in China based on a standardized precipitation and evapotranspiration index and multiple GCMs. *Sci. Total Environ.* **2019**, *704*, 135245. [CrossRef]

9. Yao, N.; Li, Y.; Lei, T.; Peng, L. Drought evolution, severity and trends in mainland China over 1961–2013. *Sci. Total Environ.* **2018**, *616–617*, 73–89. [CrossRef]

10. Beguería, S.; Vicente-Serrano, S.M.; Gracia, F.R.; Latorre, B. Standardized precipitation evapotranspiration index (SPEI) revisited: Parameter fitting, evapotranspiration models, tools, datasets and drought monitoring. *Int. J. Clim.* **2014**, *34*, 3001–3023. [CrossRef]

11. Chen, X.; Zhang, L.; Zou, L.; Shan, L.; She, D. Spatio-temporal variability of dryness/wetness in the middle and lower reaches of the Yangtze River Basin and correlation with large-scale climatic factors. *Meteorol. Atmos. Phys.* **2019**, *131*, 487–503. [CrossRef]

12. Gao, X.; Zhao, Q.; Zhao, X.; Wu, P.; Pan, W.; Gao, X.; Sun, M. Temporal and spatial evolution of the standardized precipitation evapotranspiration index (SPEI) in the Loess Plateau under climate change from 2001 to 2050. *Sci. Total Environ.* **2017**, *595*, 191–200. [CrossRef] [PubMed]

13. Polong, F.; Chen, H.; Sun, S.; Ongoma, V. Temporal and spatial evolution of the standard precipitation evapotranspiration index (SPEI) in the Tana River Basin, Kenya. *Theor. Appl. Climatol.* **2019**, *138*, 777–792. [CrossRef]

14. Vicente-Serrano, S.M.; Beguería, S.; López-Moreno, J.I. A Multiscalar Drought Index Sensitive to Global Warming: The Standardized Precipitation Evapotranspiration Index. *J. Clim.* **2010**, *23*, 1696–1718. [CrossRef]

15. Zhang, Q.; Kong, D.; Singh, V.P.; Shi, P. Response of vegetation to different time-scales drought across China: Spatiotemporal patterns, causes and implications. *Glob. Planet. Chang.* **2017**, *152*, 1–11. [CrossRef]

16. Bordi, I.; Fraedrich, K.; Jiang, J.; Sutera, A. Spatio-temporal variability of dry and wet periods in eastern China. *Theor. Appl. Climatol.* **2004**, *79*, 81–91. [CrossRef]

17. Hayes, M.J.; Svoboda, M.D.; Wilhite, D.A.; Vanyarkho, O.V. Monitoring the 1996 Drought Using the Standardized Precipitation Index. *Bull. Am. Meteorol. Soc.* **1999**, *80*, 429–438. [CrossRef]

18. Guo, H.; Bao, A.; Liu, T.; Jiapaer, G.; Ndayisaba, F.; Jiang, L.; Kurban, A.; De Maeyer, P. Spatial and temporal characteristics of droughts in Central Asia during 1966–2015. *Sci. Total Environ.* **2018**, *624*, 1523–1538. [CrossRef]

19. Allen, R.G. Crop Evapotranspiration-Guidelines for computing crop water requirements. FAO Irrigation and Drainage Paper. **2006**.

20. Vicente-Serrano, S.M.; Lopez-Moreno, I.; Gimeno, L.; Nieto, R.; Morán-Tejeda, E.; Lorenzo-Lacruz, J.; Beguería, S.; Azorin-Molina, C. A multiscalar global evaluation of the impact of ENSO on droughts. *J. Geophys. Res.* **2011**, *116*, D20109. [CrossRef]

21. Chen, X.; Li, C.; Li, X.; Yang, M.; Li, L. Modulation of the impacts of Madden–Julian Oscillation on winter rainfall in China by El Niño-Southern Oscillation. *Int. J. Climatol.* **2020**, *40*, 4039–4052. [CrossRef]

22. Yuan, Y.; Yang, H.; Zhou, W.; Li, C. Influences of the Indian Ocean dipole on the Asian summer monsoon in the following year. *Int. J. Climatol.* **2008**, *28*, 1849–1859. [CrossRef]

23. Ding, Y. *Chinese Meteorological Disasters Pandect*; China Meteorological Press: Beijing, China, 2008. (In Chinese)

24. Helsel, D.R.; Hirsch, R.M. *Statistical Methods in Water Resources*; Elsevier: Amsterdam, The Netherlands, 1992.

25. Allen, R.G.; Pereira, L.S.; Raes, D.; Smith, M. *Crop Evapotranspiration. Guidelines for Computing Crop Water Requirements*; FAO Irrigation and Drainage Paper No. 56; FAO: Rome, Italy, 1998.

26. Li, S.; Wang, Z.; Fan, S.; Wang, B.; Xu, C. Analysis of temporal-spatial variation and climate influencing factors on wine grape water requirement in Gansu province during the past 30 years. *Northen Hortic.* **2015**, *10*, 190–195.

27. Singh, V.P.; Guo, H.; Yu, F.X. Parameter estimation for 3-parameter log-logistic distribution (LLD3) by Pome. *Stoch. Hydrol. Hydraul.* **1993**, *7*, 163–177. [CrossRef]

28. Lee, S.H.; Yoo, S.H.; Choi, J.Y.; Bae, S. Assessment of the Impact of Climate Change on Drought Characteristics in the Hwanghae Plain, North Korea Using Time Series SPI and SPEI: 1981–2100. *Water* **2017**, *9*, 579. [CrossRef]

29. Montaseri, M.; Amirataee, B. Comprehensive stochastic assessment of meteorological drought indices. *Int. J. Climatol.* **2017**, *37*, 998–1013. [CrossRef]

30. Hamed, K.H.; Rao, A.R. A modified Mann-Kendall trend test for autocorrelated data. *J. Hydrol.* **1998**, *204*, 182–196. [CrossRef]

31. Kendall, M.G. *Rank Correlation Methods*; Charles Grifin: London, UK, 1975.

32. Mann, H.B. Nonparametric tests against trend. *Econom. J. Econom. Soc.* **1945**, *13*, 245–259. [CrossRef]

33. Hu, W.; Si, B.C. Technical note: Multiple wavelet coherence for untangling scale-specific and localized multivariate relationships in geosciences. *Hydrol. Earth Syst. Sci.* **2016**, *20*, 3183–3191. [CrossRef]

34. Hu, W.; Si, B.C.; Biswas, A.; Chau, H.W. Temporally stable patterns but seasonal dependent controls of soil water content: Evidence from wavelet analyses. *Hydrol. Process.* **2017**, *31*, 3697–3707. [CrossRef]

35. Grinsted, A.; Moore, J.C.; Jevrejeva, S. Application of the cross wavelet transform and wavelet coherence to geophysical time series. *Nonlinear Process. Geophys.* **2004**, *11*, 561–566. [CrossRef]

36. Kumar, P.; Foufoula-Georgiou, E. Wavelet analysis for geophysical applications. *Rev. Geophys.* **1997**, *35*, 385–412. [CrossRef]

37. Torrence, C.; Compo, G.P. A practical guide to wavelet analysis. *Bull. Am. Meteorol. Soc.* **1998**, *79*, 61–78. [CrossRef]

38. Graf, A.; Bogena, H.R.; Drüe, C.; Hardelauf, H.; Pütz, T.; Heinemann, G.; Vereecken, H. Spatiotemporal relations between water budget components and soil water content in a forested tributary catchment. *Water Resour. Res.* **2014**, *50*, 4837–4857. [CrossRef]

39. Mullon, L.; Chang, N.-B.; Yang, Y.J.; Weiss, J. Integrated remote sensing and wavelet analyses for screening short-term teleconnection patterns in northeast America. *J. Hydrol.* **2013**, *499*, 247–264. [CrossRef]

40. Perez-Valdivia, C.; Sauchyn, D.; Vanstone, J. Groundwater levels and teleconnection patterns in the Canadian Prairies. *Water Resour. Res.* **2012**, *48*, 7516. [CrossRef]

41. Rashid, M.; Beecham, S.; Chowdhury, R.K. Assessment of trends in point rainfall using Continuous Wavelet Transforms. *Adv. Water Resour.* **2015**, *82*, 1–15. [CrossRef]

42. Torrence, C.; Webster, P.J. Interdecadal changes in the ENSO–monsoon system. *J. Clim.* **1999**, *12*, 2679–2690. [CrossRef]

43. Guttman, N.B. Accepting The Standardized Precipitation Index: A Calculation Algorithm. *J. Am. Water Resour. Assoc.* **1999**, *35*, 311–322. [CrossRef]

44. Wei, X.; Hu, Q.; Ma, X.; Zheng, S.; Tang, X.; Zhang, Y.; Pan, X.; He, Q. Temporal-spatial variation characteristics of drought in summer maize growing season in north China plain based on SPEI. *J. Arid Meteorol.* **2018**, *36*, 554–560.

45. Xu, L.; Wang, H.; Duan, Q.; Ma, J. The temporal and spatial distribution of droughts during summer corn growth in yunnan Province based on SPEI. *Resour. Sci.* **2013**, *35*, 1024–1034.

46. Yan, Y.; Li, Z. Temporal and spatial variation characteristics of drought trend at growth stage of winter wheat in Henan province based on SPEI index. *J. Nanjing Univ. Inf. Sci. Technol. Nat. Sci. Ed.* **2015**, *7*, 159–167.

47. Cook, B.I.; Smerdon, J.E.; Seager, R.; Coats, S. Global warming and 21st century drying. *Clim. Dyn.* **2014**, *43*, 2607–2627. [CrossRef]

48. Vicente-Serrano, S.M.; Van der Schrier, G.; Beguería, S.; Azorin-Molina, C.; Lopez-Moreno, J.-I. Contribution of precipitation and reference evapotranspiration to drought indices under different climates. *J. Hydrol.* **2015**, *526*, 42–54. [CrossRef]

49. Wang, Z.; Li, J.; Lai, C.; Zeng, Z.; Zhong, R.; Chengguang, L.; Zhou, X.; Wang, M. Does drought in China show a significant decreasing trend from 1961 to 2009? *Sci. Total Environ.* **2017**, *579*, 314–324. [CrossRef] [PubMed]

50. Zhai, J.; Su, B.; Krysanova, V.; Vetter, T.; Gao, C.; Jiang, T. Spatial Variation and Trends in PDSI and SPI Indices and Their Relation to Streamflow in 10 Large Regions of China. *J. Clim.* **2010**, *23*, 649–663. [CrossRef]

51. Dahlstrom, R. *Desert Problems and Desertification in Central Asia*; Springer: Berlin, Germany; London, UK, 2012.

52. Wu, X. *Analysis of Thermal Conditions and Climatic Regionalization of Grape Planting in China Based on km Grid*; Shenyang Agricultural University: Shenyang, China, 2019.

53. Liu, D.; Zhu, B.; Dong, A.; Qu, W. Characteristics and reasons of drought in Gansu province in 2001. *Gansu Meteor.* **2002**, *20*, 4–7.

54. Du, S.; Cheng, X.; Huang, Q.; Chen, R.; Ward, P.J.; Aerts, J.C.J.H. Brief communication: Rethinking the 1998 China floods to prepare for a nonstationary future. *Nat. Hazards Earth Syst. Sci.* **2019**, *19*, 715–719. [CrossRef]

55. Lu, B.; Ren, H.-L. Improving ENSO periodicity simulation by adjusting cumulus entrainment in BCC_CSMs. *Dyn. Atmos. Oceans* **2016**, *76*, 127–140. [CrossRef]

56. MacMynowski, D.G.; Tziperman, E. Factors affecting ENSO's period. *J. Atmos. Sci.* **2008**, *65*, 1570–1586. [CrossRef]

57. Li, C.; Zhao, T. Seasonal responses of precipitation in China to El Niño and positive Indian ocean dipole modes. *Atmosphere* **2019**, *10*, 372. [CrossRef]

58. Qiu, Y.; Cai, W.; Guo, X.; Ng, B. The asymmetric influence of the positive and negative IOD events on China's rainfall. *Sci. Rep.* **2015**, *4*, 4943. [CrossRef]

59. Weng, H.; Wu, G.; Liu, Y.; Behera, S.K.; Yamagata, T. Anomalous summer climate in China influenced by the tropical Indo-Pacific Oceans. *Clim. Dyn.* **2011**, *36*, 769–782. [CrossRef]

60. Xu, K.; Zhu, C.; Wang, W. The cooperative impacts of the El Niño-Southern Oscillation and the Indian Ocean Dipole on the interannual variability of autumn rainfall in China. *Int. J. Climatol.* **2016**, *36*, 1987–1999. [CrossRef]

61. Xiao, M.; Zhang, Q.; Singh, V.P. Spatiotemporal variations of extreme precipitation regimes during 1961–2010 and possible teleconnections with climate indices across China. *Int. J. Climatol.* **2016**, *37*, 468–479. [CrossRef]